

# Geochemistry, Geophysics, Geosystems

## RESEARCH ARTICLE

10.1029/2020GC009150

### Key Points:

- Variations in lithosphere thickness exert first-order control on continental elevations, defining whole lithosphere isostasy (WLI)
- WLI explains most elevations for lithospheric mantle density contrasts with crust and asthenosphere of 300 to 550 and 20 to 40 kg m<sup>-3</sup>
- Elastic thickness is typically 25% to 50% of the thickness of the conductive lithosphere, with a mode of 35%

### Supporting Information:

- Supporting Information S1
- Figure S1
- Data Set S1

### Correspondence to:

S. Lamb,  
simon.lamb@vuw.ac.nz

### Citation:

Lamb, S., Moore, J. D. P., Perez-Gussinye, M., & Stern, T. (2020). Global whole lithosphere isostasy: Implications for surface elevations, structure, strength, and densities of the continental lithosphere. *Geochemistry, Geophysics, Geosystems*, 21, e2020GC009150. <https://doi.org/10.1029/2020GC009150>

Received 1 MAY 2020

Accepted 14 SEP 2020

Accepted article online 23 SEP 2020

## Global Whole Lithosphere Isostasy: Implications for Surface Elevations, Structure, Strength, and Densities of the Continental Lithosphere

Simon Lamb<sup>1</sup> , James D. P. Moore<sup>1,2</sup> , Marta Perez-Gussinye<sup>3</sup> , and Tim Stern<sup>1</sup> 

<sup>1</sup>Institute of Geophysics, SGEES, Victoria University of Wellington, Wellington, New Zealand, <sup>2</sup>Earth Observatory of Singapore, Nanyang Technological University of Singapore, Singapore, <sup>3</sup>MARUM—Center for Marine Environmental Sciences, University of Bremen, Bremen, Germany

**Abstract** The observed variations in the thickness of the conductive lithosphere, derived from surface wave studies, have a first-order control on the elevation of the continents, in addition to variations in the thickness of the crust—this defines whole lithosphere isostasy (WLI). Negative buoyancy of the mantle lithosphere counters the positive buoyancy of the crust, and together, their respective thicknesses and density contrasts determine elevation of the continents both in their interiors and at their edges. The average density contrasts for lithospheric mantle with crust and with asthenosphere are typically 300 to 550 and 20 to 40 kg m<sup>-3</sup>, respectively, with a ratio 10 to 16, suggesting moderate average depletion of lithospheric mantle. We show that a crustal model for Antarctica, assuming WLI and using these density contrasts, provides a close fit to estimates of crustal thickness from surface wave tomography and gravity observations. We use a global model of WLI as a framework to assess factors controlling topography, showing that plausible regional variations in crustal and mantle densities, together with uncertainties in the crustal and conductive lithospheric thicknesses, are sufficient to account for global elevations without invoking dynamic topography greater than a few hundred meters. Estimates of elastic thickness  $T_e$  in the continents are typically 25–50% of the thickness of the conductive lithosphere, indicating that the mantle part supports some of the elastic strength of the lithosphere.

## 1. Introduction

Isostasy exerts a fundamental control on the elevation of the continents, determined by the density structure of the lithosphere and asthenosphere. The largest density contrast in the continental lithosphere is at the Moho, and so it is widely assumed that crustal thickness is the principal factor determining surface heights, as originally proposed by George Airy (Airy, 1855). At the time that Airy published his ideas on isostasy, the thickness and nature of the crust and mantle were unknown. It is likely that Airy's ideas stemmed from his work on the average density of the Earth, based on the gradient of gravity down deep mine shafts (Airy, 1856), presumably prompting the idea at the heart of Airy isostasy of a light outer layer of crust “floating” on a denser interior. In simple Airy Isostasy, floatational equilibrium is assumed to occur at the base of the thickest crust, defined as the depth of compensation (Figure 1a). In this case, variations in elevation ( $\Delta H$ , increase is positive) of the Earth's surface above sea level are determined by both variations in crustal thickness ( $\Delta C$ , increase is positive) and the densities of the crust ( $\rho_c$ ) and mantle ( $\rho_m$ ):

$$\Delta H = \Delta C / \alpha', \quad (1)$$

where  $\alpha' = \rho_m / (\rho_m - \rho_c)$ . For typical mantle and crustal densities (Christensen & Mooney, 1995; Ludwig et al., 1970), this indicates that  $\alpha'$  is in the range 5–8, corresponding to a crust-mantle density contrast in the range 400–600 kg m<sup>-3</sup>. We can correct for water depth by multiplying the right-hand side of Equation 1 by a factor  $\rho_m / (\rho_m - \rho_w)$ , where  $\rho_w$  is the density of water.

With the development of plate tectonic theory, it has become clear that the crust and the top few tens to hundreds of kilometers of the underlying mantle comprise a relatively “cool” lithosphere that in the oceans, at least, rests on a hotter and weaker asthenosphere. Here, we are defining the base of the lithosphere in terms of the thermal structure of the outer part of the Earth, effectively marking a change from a conductive to convective cooling regime—we call this the conductive lithosphere. We note that the base of the conductive

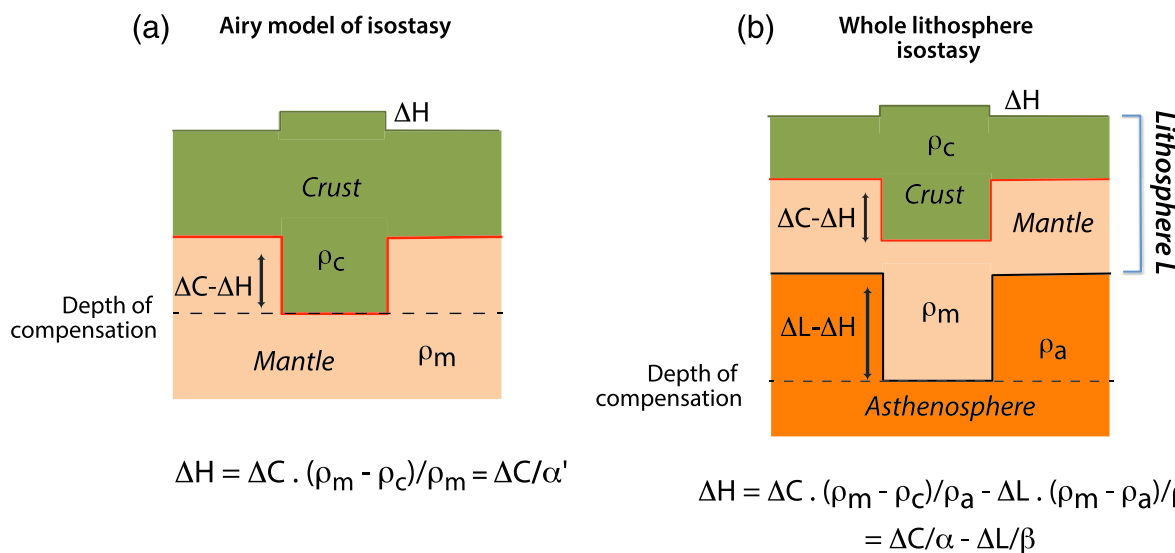


**Figure 1.** Models of local isostasy. (a) Simple Airy isostasy in which the crust is in flotation equilibrium with the underlying lithospheric mantle, with a depth of compensation at the base of the crust. In this case, a change in surface elevation  $\Delta H$  is directly proportional to the change  $\Delta C$  in underlying crustal thickness. (b) Whole lithosphere isostasy in which the lithosphere is in flotation equilibrium with the underlying asthenosphere, with a depth of compensation at the base of the lithosphere. In this case, a change in surface elevation is linearly related to both the change in underlying crustal and lithospheric  $\Delta L$  thickness.

lithosphere is not necessarily the same as the LAB imaged from receiver functions, seismic tomography, and reflection and refraction seismology (Fischer et al., 2010; Kind et al., 2012; Stern et al., 2015). The “cooler” conductive lithospheric mantle would be predicted to be more dense than the underlying asthenosphere. In the continents, however, it has been proposed that the lithospheric mantle is significantly depleted due to melt extraction compared to asthenospheric mantle beneath the mid-ocean ridge, based on theoretical arguments of mantle melting and direct observation of mantle xenoliths, and this depletion will act to reduce or even reverse this density contrast (Crosby et al., 2010; Jordan, 1975, 1978, 1988; McKenzie, 1989; Naliboff et al., 2012).

The relative plate motions between continental plates are generally accommodated in plate boundary zones that are hundreds to thousands of kilometers wide, leading to both crustal and lithospheric thinning and thickening. Thus, implicit in the theory of plate tectonics is the concept of at least two regional density contrasts in the outer relatively “cold” and “strong” part of the Earth, between the crust and mantle, and between the lithospheric and asthenospheric mantle; and both crust and lithosphere are likely to show significant lateral variations in thickness. This way, the concept of Airy isostasy in the continents has been logically extended to include the whole lithosphere (Figure 1b; Becker et al., 2014; Crosby et al., 2010; Gvirtzman et al., 2016; Molnar et al., 2015; Naliboff et al., 2012), referred to here as whole lithosphere isostasy (WLI), as has been done so successfully in the oceans (Figure 1b; Parsons & McKenzie, 1978; Parsons & Sclater, 1977). However, in the presence of significant flexural strength of the lithosphere, this isostatic balance will be regional (i.e., hundreds of kilometers scale) rather than local (Watts, 2001).

The thickness of the conductive lithosphere has been until recently poorly constrained. Also, the average density contrast between lithospheric and asthenospheric mantle will be much smaller than that with the crust because it is principally controlled by temperature and further reduced by depletion—a key problem is quantifying the crust, mantle, and asthenosphere density contrasts. If the product of conductive lithosphere mantle thickness with its density contrast to the underlying asthenosphere is very small, then simple Airy isostasy (assuming compensation at the base of the crust) may be a good enough approximation for most regional analyses of the elevations in the continents. However, quantifying buoyancy of the lithospheric mantle is essential for modeling rift basins or continental margins (Allen & Allen, 2013; McKenzie, 1978). In addition, it has been hypothesized that drastic changes in lithospheric thickness due to delamination or Rayleigh-Taylor instabilities, as a consequence of the negative buoyancy of the lithospheric mantle, may be an important mechanism of surface uplift (Bird & Baumgardner, 1981; England &

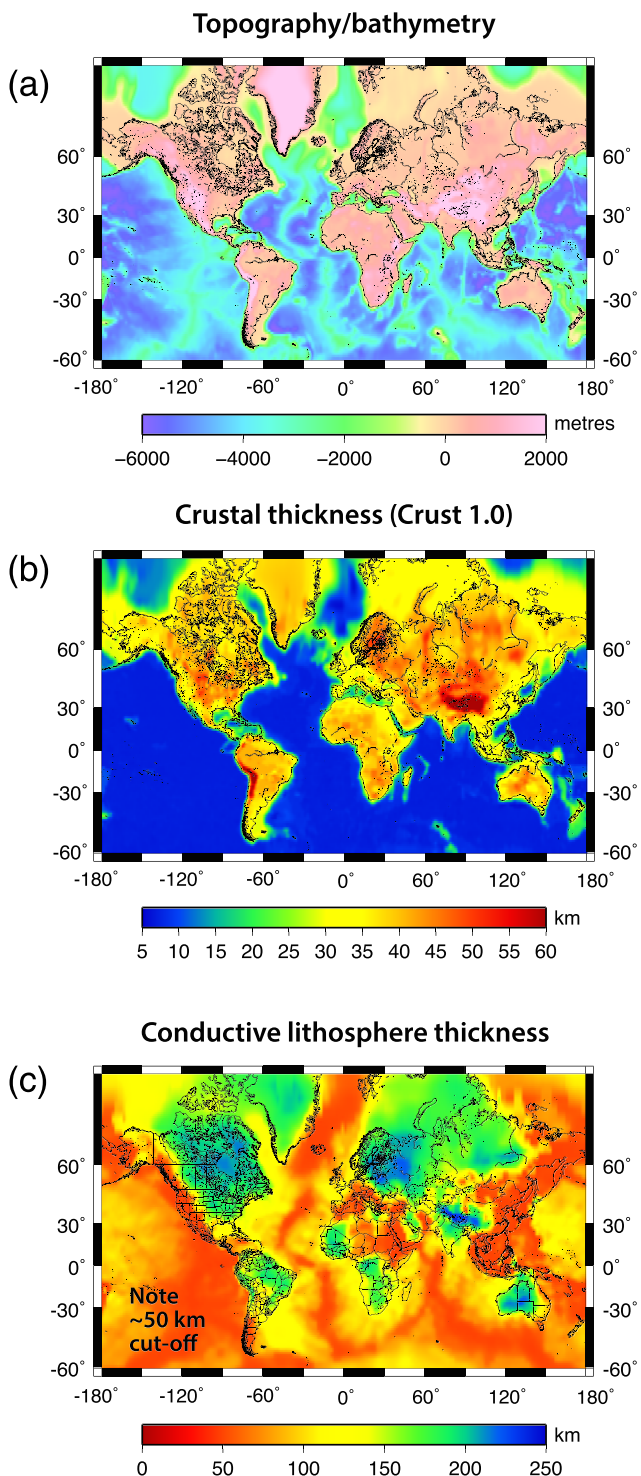


**Figure 2.** Global data for isostatic models. (a) Surface topography/bathymetry from ETOPO1 (2011). (b) Crustal thickness from CRUST 1.0 (Laske et al., 2013). (c) Lithospheric thickness from seismic surface wave/thermal model of Priestley et al. (2019)—note lower cutoff at about 50 km where lithospheric thickness becomes poorly resolved.

Houseman, 1989; Houseman & England, 1986; Houseman et al., 1981; Houseman & Molnar, 1997; Hyndman & Currie, 2011; Molnar et al., 1993; Platt & England, 1994). This could explain the greater elevation of the North American Cordillera compared to the continental interior, despite the fact that the crust is thinner beneath the Cordillera (Hyndman & Currie, 2011). Indeed, it may be Rayleigh-Taylor instabilities that smooth out variations in lithospheric thickness (England & Houseman, 1986). It has also been argued that flow stresses in the asthenosphere may be sufficient to significantly change the isostatic balance, giving rise to dynamic topography, although this is the subject of controversy—see Molnar et al. (2015) for a review of the role of dynamic topography. Finally, where there have been recent changes in loading of the lithosphere due to melting of large ice sheets, the state of isostatic balance may be in transition to a new state on timescales of tens of thousands of years, giving rise to postglacial rebound, although these elevation changes will not have more than a few hundred meters to go in the future (Ranalli, 1995; Whitehouse, 2018).

We explore the implications of WLI for the elevations, lithospheric structure, densities, and strength of the continents. Our approach has similarities to that of previous authors (Becker et al., 2014; Gvirtzman et al., 2016; Hyndman & Currie, 2011; Naliboff et al., 2012), but applied globally, and it is a simplified form of thermal isostasy (Hasterok & Chapman, 2007a, 2007b), reexpressed in terms of lateral variations in lithospheric thickness rather than thermal structure.

### 1.1. WLI

A simple way to assess the role of WLI in determining the surface elevations of the continents is to compare crustal thickness with elevation, in order to determine how elevation departs from that predicted by simple Airy isostasy in Equation 1. We use global data sets regridded at  $1 \times 1^\circ$  to compute both grid point values and average values of elevation (ETOPO1, 2011, <https://www.ngdc.noaa.gov/mgg/global/>), and crustal thickness (CRUST 1.0, Laske et al., 2013, <https://igppweb.ucsd.edu/~gabi/crust1.html>)—see Figure 2. We calculate average values for individual continental interiors (Figure 3a), using updated crustal data for Antarctica (Shen et al., 2018) and Zealandia (Lamb et al., 2015). These are simply calculated by multiplying the value in each grid square by its area and then summing over the region of interest and dividing by the total area of the particular continental region (thousands of kilometers across).

It is clear that when elevation (corrected where appropriate for water depth) is plotted against crustal thickness, then over the full range of crustal thickness (5–80 km), there is a broad positive correlation as might be predicted by simple Airy isostasy (Figure 3b). But over a smaller range of crustal thickness this correlation clearly breaks down, particularly for typical continental crust in the range 25 and 50 km thick. Here, elevation appears to be only weakly sensitive to crustal thickness, implying a mantle-crust density contrast  $<200 \text{ kg m}^{-3}$ —we refer to this discrepancy in continental crust as the Airy “failure” (Figure 3b). This cannot be ascribed to the effects of lithospheric flexure, as it is apparent over length scales of

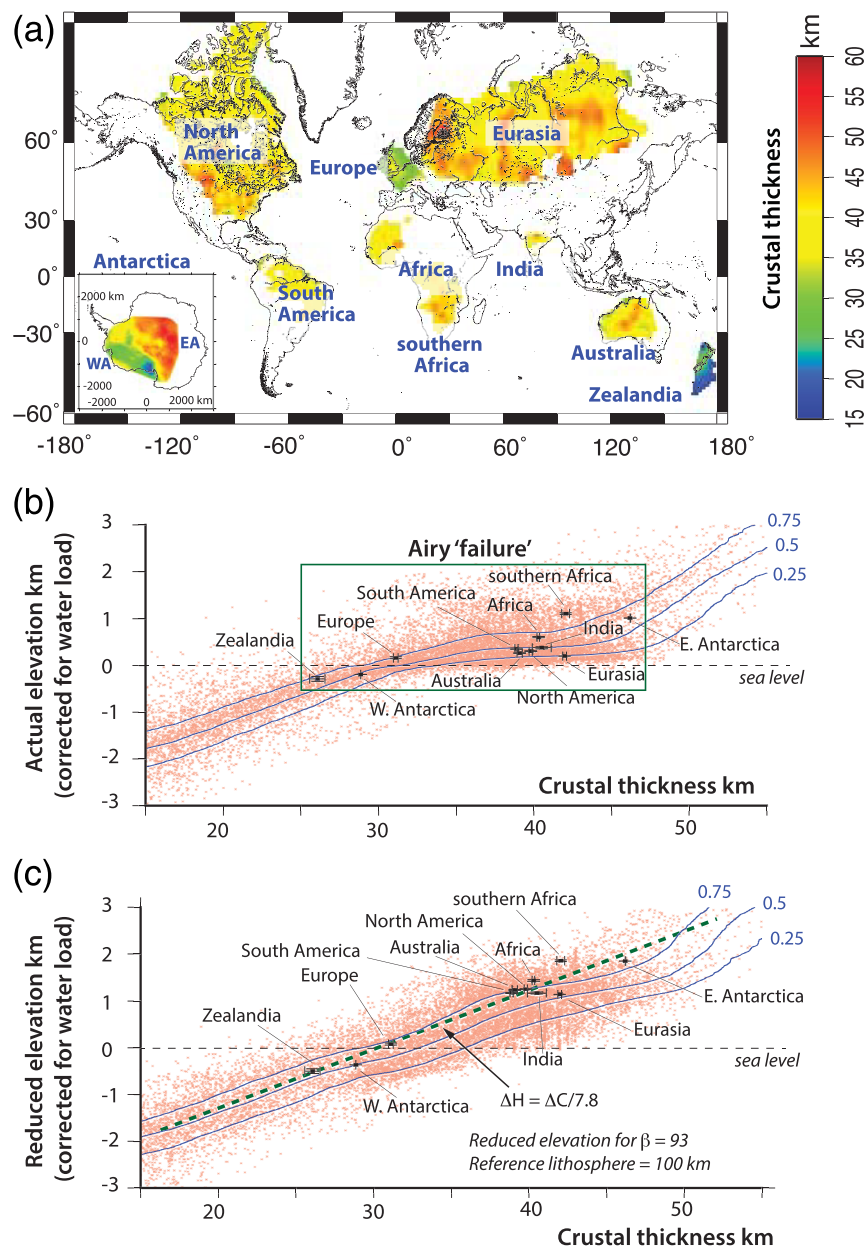


**Figure 3.** (a) Continental regions defined in this study, using CRUST 1.0 for Europe and continental interiors (conductive lithosphere >150 km, Priestley et al., 2019) of North America, South America, Eurasia, Australia, Africa, and India (see b and c). Inset map shows crustal structure of part of Antarctica (EA = East Antarctica; WA = West Antarctica) after Shen et al. (2018). Crustal compilation from Lamb et al. (2015) used for Zealandia. (b) Plot of crustal thickness (see Figure 2b) against elevation (see Figure 2a), either for individual  $1 \times 1^\circ$  grid squares (red crosses) or continental averages, as defined in (a). Regions below sea level are corrected for water load (see text). Although there is a broad correlation between elevation and crustal thickness, as predicted by simple Airy isostasy (Figure 1a), these are only weakly related for crustal thicknesses between 25 and 50 km, giving rise to the so-called Airy "failure." Also shown are contours of 0.25, 0.5, and 0.75 quartiles of number of observations for any particular conductive lithosphere thickness—0.5 contour defines median of data. (c) Crustal thickness of continents, as in (b), plotted against reduced elevation corrected for both water load and lithospheric thickness. Quartile contours as in (b). The reduced elevation is the elevation that a continent would have assuming whole lithosphere isostasy (WLI) for a 100 km lithospheric thickness and a lithospheric mantle/asthenosphere density contrast of  $35 \text{ kg m}^{-3}$ . The plot now fits well to a straight line, with  $R^2 = 0.943$ , with a slope implying typical conductive lithospheric mantle-crust density contrast of  $417 \text{ kg m}^{-3}$ , for a reference asthenospheric density of  $3,250 \text{ kg m}^{-3}$  (equivalent to  $\alpha = 7.8$ ). This shows that WLI is a very good approximation for the continents at hundreds of kilometers length scale, requiring regionally negative buoyancy mantle lithosphere.

thousands of kilometers, and much greater than is likely to be supported by flexure for plausible values of  $T_e$  (McKenzie & Fairhead, 1997; Watts, 2001). For the same reasons, it is difficult to explain in terms of systematic errors in crustal models, unless continental-scale crustal studies show significant bias of up to 10 km in thickness determinations.

Molnar et al. (2015) argue that because regional free air and isostatic gravity anomalies in the continents are generally less than a few tens of milligals, the contribution to topography of normal flow stresses arising from asthenospheric flow can be no more than a few hundred meters—which they call dynamic topography. In agreement with this, we demonstrate in the following sections that the Airy “failure” in the continents can largely be explained by the isostatic effect of observed variations in conductive lithospheric thickness, together with plausible variations in crustal and mantle densities.

Priestley and McKenzie (2013) mapped out the thickness of the conductive lithosphere in the continents from inversions of a broad spectrum of seismic surface waves, although their methodology cannot resolve lithospheric thickness much less than about 50 km. An updated version of their lithospheric model was made available (<http://ds.iris.edu/ds/products/emc-cam2016/>), which we use in this study, referred to as Priestley et al. (2019). The base of the conductive lithosphere here is defined by the depth at which the conductive geotherm intersects the convective geotherm, using a calibration between  $S$ -wave velocity and pressure and temperature based on mantle xenoliths and a plate cooling model for oceanic lithosphere—see Priestley and McKenzie (2006); Priestley and McKenzie (2013) for a full description of their methodology. This is more or less an isotherm, between 1350°C and 1400°C, depending on the precise conductive and convective geotherms (Priestley & McKenzie, 2013). The resolution of the model is about 250 km horizontally, with a vertical uncertainty of ~30 km, but the locus of gradients of lithospheric thickness is more precisely determined, although flattened by the moving window method of averaging (Priestley & McKenzie, 2013).

Priestley et al.’s (2019) analysis has revealed significant variation in the thickness of the conductive lithosphere. In the oceans, the conductive lithosphere progressively thins from about 120 km thick beneath old ocean floors to <50 km beneath the mid-ocean ridges. In the continents, the conductive lithosphere seems to vary in thickness by up to 200 km, reaching depths up to 250 km, depending on the crustal geological evolution, with thick lithosphere beneath the continental interiors and thinner lithosphere beneath younger mobile belts and rift zones (McKenzie et al., 2015; Priestley & McKenzie, 2013; Priestley et al., 2019). This image of the conductive lithosphere largely conforms with previous estimates based on heat flow, thermal structure, and mantle xenoliths (Chapman & Pollack, 1977; McKenzie et al., 2005; Pollack & Chapman, 1977; Priestley & McKenzie, 2013; Priestley et al., 2019).

If we assume a simple three-layer crust, lithospheric mantle, and asthenosphere structure, with a depth of compensation in the asthenosphere (Figure 1b), then for WLI, the factors controlling changes in surface elevation above sea level ( $\Delta H$ ) will include, in addition to those of simple Airy isostasy (Equation 1), changes in lithospheric thickness ( $\Delta L$ , increase is positive), and the density of the asthenospheric mantle ( $\rho_a$ ), where  $\rho_m$  is now the *average* density of the lithospheric mantle:

$$\Delta H = \Delta C/a - \Delta L/\beta, \quad (2)$$

where  $\alpha = \rho_a/(\rho_m - \rho_c)$  and  $\beta = \rho_a/(\rho_m - \rho_a)$ , and water depth is allowed for by multiplying the right-hand side of Equation 2 by a factor  $\rho_a/(\rho_a - \rho_w)$ . Note that we would anticipate the local density of the lithospheric mantle to decrease with depth as the temperature increases, although perturbed by depletion effects (Crosby et al., 2010; Naliboff et al., 2012). However, the total range in density will be small and <3% of the actual density given typical coefficients of expansion and lithospheric mantle temperatures (McKenzie et al., 2005); the critical parameters in Equation 2 are the average density contrasts between the lithospheric mantle and crust ( $\rho_m - \rho_c$ ) and asthenospheric mantle ( $\rho_m - \rho_a$ ). For negatively buoyant mantle lithosphere, an increase/decrease in lithospheric thickness has the opposite effect on elevation to an increase/decrease in crustal thickness. Supporting information Figure S1 shows values of  $\alpha$  and  $\beta$  plotted against the corresponding density contrasts of conductive lithosphere with crust and asthenosphere, for a reference asthenospheric density of  $3,250 \text{ kg m}^{-3}$ —note that the density contrasts are very insensitive to the choice of reference density, given particular values of  $\alpha$  and  $\beta$ .

## 1.2. Constraining Lithospheric Density Contrasts

The parameters  $\alpha$  and  $\beta$  in Equation 2 determine the relation between lithospheric and crustal thickening. But because these two processes usually have opposite effects (for  $\rho_m > \rho_a$  and  $\rho_m > \rho_c$ ) on topography, and crustal thickness is often roughly correlated with lithospheric thickness in continental interiors, their ratio is better constrain than their individual values. This is easy to see if one considers a region of subdued topography. In this case  $\Delta C/\alpha \sim \Delta L/\beta$ , for negatively buoyant mantle lithosphere, or  $\beta/\alpha = \Delta L/\Delta C$ . Figure 4a shows a plot of conductive lithospheric thickness against crustal thickness for elevations within 50 m of sea level. Thus, the slope of the plot gives  $\beta/\alpha \sim 15$ . We can also use this plot to define a reference lithospheric structure that is at sea level. If we take a lithospheric thickness of 100 km, then the reference crustal thickness for sea level is  $\sim 32$  km (Figure 4a). In theory, choosing an elevation that is not sea level should yield  $\alpha$  and  $\beta$  individually from the slope and intercept of the plot, but this requires the crustal and lithospheric thicknesses to be known with high precision. The effects of any error in these, together with variations in crustal and mantle densities, will be amplified for low values of  $\alpha$  and  $\beta$  (i.e., high values of their *reciprocals* that determine the isostatic balance in Equation 2) because we are assessing the difference of two large numbers. Thus, the best fit solution tends to be strongly biased toward high values of  $\alpha$  and  $\beta$  (i.e., low values of their reciprocals) even if their ratio remains more or less constant, because in this case, the uncertainty in the elevation is now the difference of two smaller numbers.

The previous discussion shows that simple minimization is not always the best way to determine values of  $\alpha$  and  $\beta$ , for example, by finding pairs of  $\alpha$  and  $\beta$  that minimize the difference between the observed and predicted elevations—referred to as the elevation anomaly—although their ratio may be well constrained. Note that we make a small isostatic adjustment to the elevation anomaly to take into account thick sedimentary basins, as compiled in the CRUST 1.0 model, assuming a sedimentary rock density here of  $2,600 \text{ kg m}^{-3}$  at depths shallower than 5 km and  $2,700 \text{ kg m}^{-3}$  for greater depths. Figure 4b shows a plot of  $\alpha$  against  $\beta$  that minimizes the average elevation anomaly, for elevations  $>-1$  km, globally (i.e., all continents). Additionally, we do the same exercise for Europe and western North America. It can be seen that the minimum elevation anomaly plots close to a line representing a ratio of  $\beta/\alpha$  in the range 10 to 16, identical to that indicated by the plot for a reference lithosphere within 50 m of sea level in Figure 4a. However, the value of  $\alpha$  that gives a minimum average elevation anomaly, both globally and for Europe, is  $\sim 16$  (Figure 4b). Taking a reference asthenospheric density of  $3,250 \text{ kg m}^{-3}$ , this translates into density contrasts for the lithospheric mantle-crust and mantle-asthenosphere of  $\sim 200$  and 10 to  $20 \text{ kg m}^{-3}$ , respectively. As we have already argued, the minimum solutions in the analyses described above can be strongly biased toward high values of  $\alpha$  and  $\beta$  (i.e., low values of the corresponding density contrasts) and may only be maximum upper bounds. For example, values typically used in gravity models are in the range 6–8.125, corresponding to mantle-crust density contrasts in the range 400 to  $550 \text{ kg m}^{-3}$ , with a typical value of  $\sim 450 \text{ kg m}^{-3}$  (Christensen & Mooney, 1995; O'Donnell & Nyblade, 2014; Tenzer & Novak, 2013; Tenzer et al., 2012). A density contrast between lithospheric mantle and crust of  $450 \text{ kg m}^{-3}$  would correspond to a contrast between lithospheric mantle and asthenosphere in the range 30 to  $40 \text{ kg m}^{-3}$ , for  $\beta/\alpha$  in the range 10 to 16.

We suggest that better ways to determine likely values of  $\alpha$  and  $\beta$  involve modeling of gravity edge effects due to steps in crustal and lithospheric thickness, combined with WLI analysis of regions with significant spatial variations in topography, and crustal and conductive lithosphere thicknesses. For example, the crust beneath New Zealand's Southern Alps, along the obliquely converging Australian-Pacific plate boundary, is determined by high-resolution seismic reflection and refraction to be up to 48 km thick, compared to about 27 km near the coast, with average surface elevations  $\sim 1.5$  km. Here, an underlying lithospheric root forming a keel-shaped structure up to 175 km thick, thickening from about 90 km on its flanks, is well imaged in a teleseismic delay experiment (Figure 5a; Bourguignon et al., 2007; Stern et al., 2000, 2007). Gravity modeling of both crustal and lithospheric roots indicates that the mantle part is negatively buoyant, with a density contrast with the asthenosphere of 30 to  $40 \text{ kg m}^{-3}$  (Figure 5a; Scherwath et al., 2006; Stern et al., 2000, 2007).

A pronounced lithospheric and crustal step is observed across the Ruapehu Taranaki line in western North Island, constrained by *P*-wave delay times, seismic refraction, and receiver functions (Figure 5b; Dimech et al., 2017; Seward, 2008; Stern et al., 1987, 2006). Both crustal and lithospheric thicknesses are less north of the step, and there is negligible topographic contrast ( $<100$  m) across the step. A pronounced edge

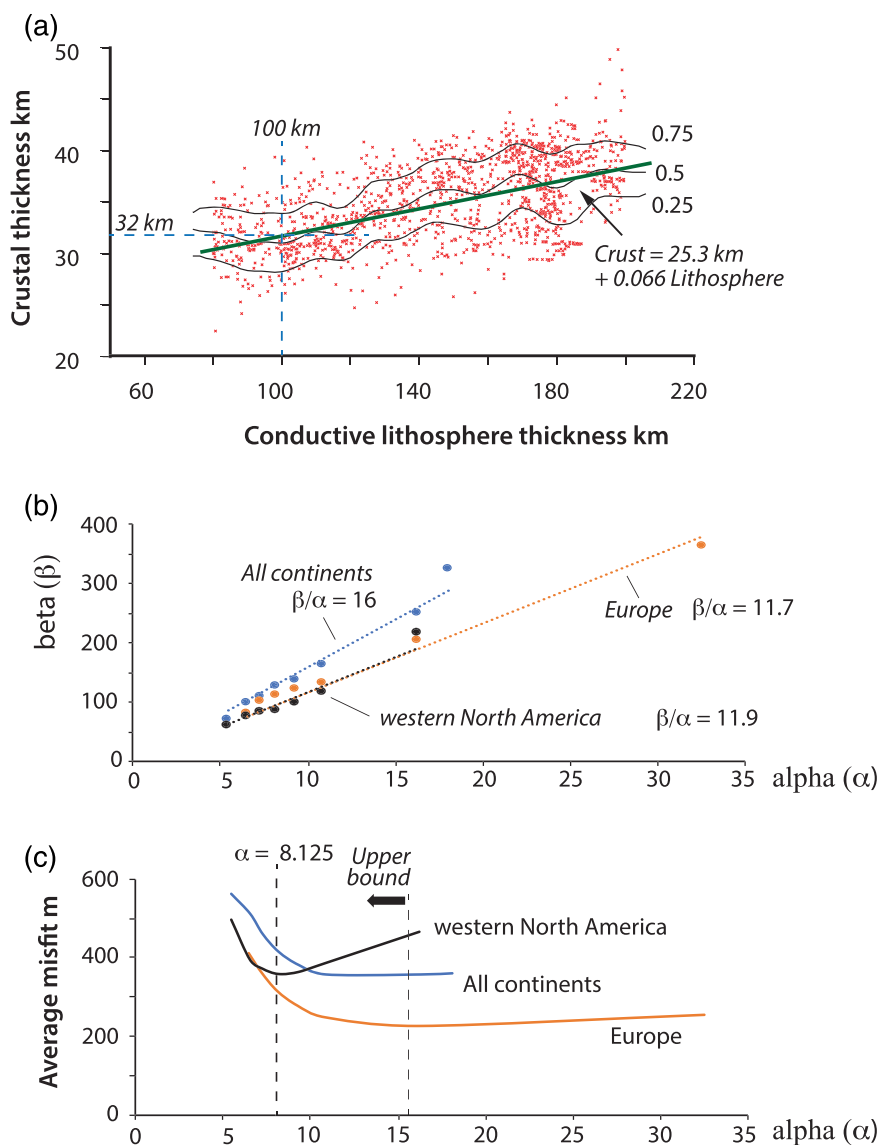


**Figure 4.** (a) Plot of conductive lithosphere against crustal thickness for elevations within 50 m of sea level, defining reference lithosphere. Crosses are for  $1^\circ$  squares, using CRUST 1.0 and Priestley et al. (2019) crustal and conductive lithosphere structure. Also shown is best fit linear fit and contours of 0.25, 0.5, and 0.75 quartiles of number of observations for any particular conductive lithosphere thickness—0.5 contour defines the median value. Note correlation between crustal and lithospheric thickness, defining average 32 km thick crust at sea level, for 100 km thick lithosphere. Linear fit gives average  $\beta/\alpha \sim 15$ , for  $\alpha$  and  $\beta$  defined in Equation 2 (see b and c and text). (b) Plots showing relation between  $\alpha$  and  $\beta$  for solution sets of minimum misfit, for “all continents” (elevations  $>-1,000$  m), “Europe,” and “western North America,” indicating a strong trade-off between  $\alpha$  and  $\beta$  but constrain their ratio in the range 10 to 16. (c) The minimum misfit solution for all solution sets is strongly biased toward high values of  $\alpha$  and  $\beta$  in regions of subdued topography in continental interiors, so it only defines upper bounds to  $\alpha$  and  $\beta$  (see text). However, the large spatial variation in elevation, crustal and conductive lithosphere thicknesses in western North America (see Figure S2) provide tighter constraints on values of  $\alpha$  and  $\beta$  individually, and not just their ratios, indicating a best fit value of  $\alpha \sim 8.125$ , corresponding to density contrasts between conductive lithosphere mantle and crust, and asthenosphere, of  $417$  and  $35 \text{ kg m}^{-3}$  ( $\beta = 93$ ), respectively.

effect gravity anomaly is associated with the step. This edge effect can be accounted for with a simple and locally compensated WLI structure and with density contrasts of 400 to 550 and 30 to 40  $\text{kg m}^{-3}$  for the lithospheric mantle with crust and with asthenosphere, respectively. A similar density contrast for lithospheric mantle with crust of 500 to 550  $\text{kg m}^{-3}$ , and 30 to 54  $\text{kg m}^{-3}$  with the underlying

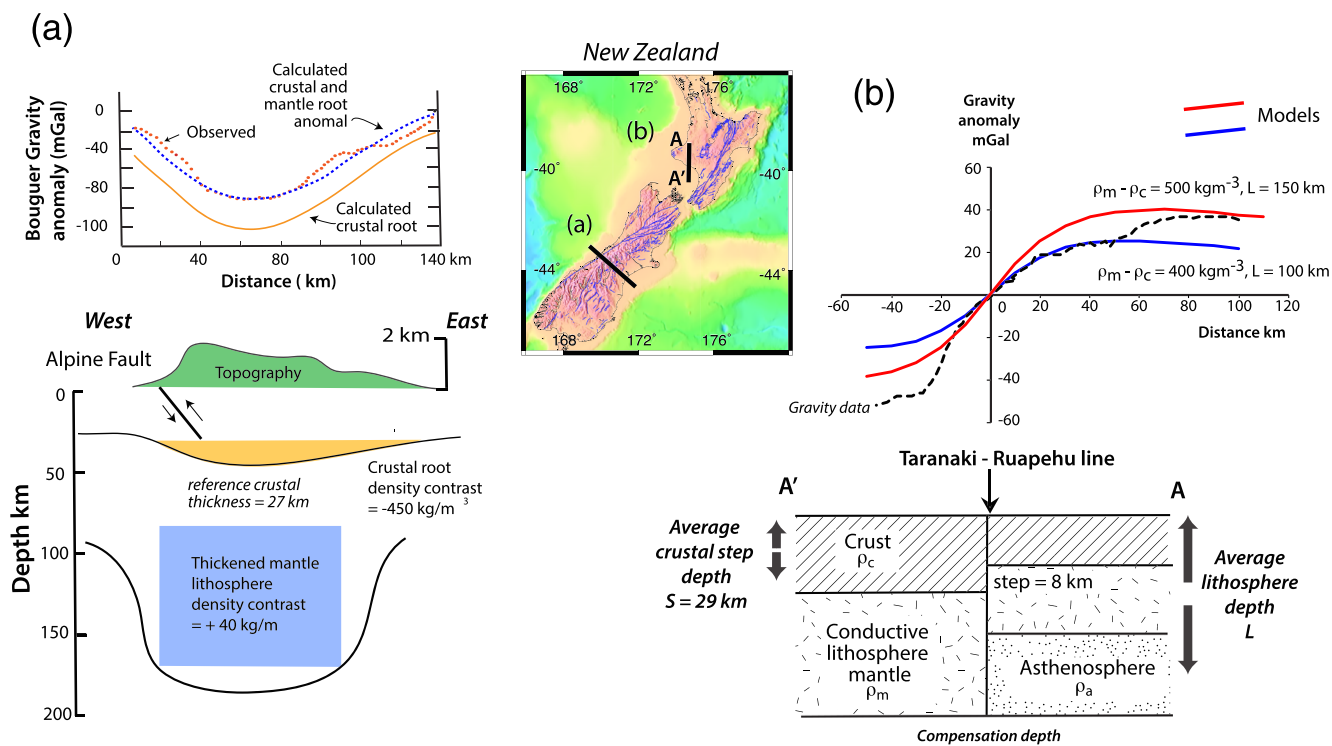


**Figure 5.** Gravity anomalies across crustal and lithospheric steps in New Zealand. (a) Gravity modeling across the Southern Alps in South Island shows that the seismically imaged lithospheric root here, up to 175 km thick (see text), is negatively buoyant with respect to the underlying asthenosphere by  $\sim 40 \text{ kg m}^{-3}$ . (b) Gravity modeling across a sharp lithospheric step in western North Island, imaged from P-wave delay times and receiver functions (see text), constrains the conductive lithosphere mantle-crust density contrast 400 to  $500 \text{ kg m}^{-3}$  ( $\alpha = 6.5$  to 8.125) and 30 to  $40 \text{ kg m}^{-3}$  with the asthenosphere ( $\beta = 81$  to 100).  $\beta/\alpha \sim 12.4$ , consistent with (a) and results from other continents (Figure 4).

asthenosphere, is also indicated by previous gravity and uplift modeling of the lithospheric step across the Transantarctic Mountains in the Ross Sea sector of Antarctica (see also section 2 and Figure 7b; Stern & ten Brink, 1989; ten Brink et al., 1997).

Western North America is a continental-scale region with significant variations in topography, and crustal and lithospheric thickness (Becker et al., 2014; Hyndman & Currie, 2011). Here the conductive lithosphere varies from over 200 km thick in the continental interior to less than 80 km farther west beneath the Cordilleras and Basin and Range province. Likewise the crust varies between  $\sim 25$  and  $\sim 50$  km thick (CRUST 1.0, Levander & Miller, 2012; Lowry & Pérez-Gussinyé, 2011). We calculate the misfit between the observed and predicted topography for the western North America in the region extending from  $30^\circ\text{N}$  to  $55^\circ\text{N}$  and  $105^\circ\text{E}$  to  $125^\circ\text{E}$ , iterating on values of  $\alpha$  and  $\beta$ , and using the standard reference lithosphere, as defined in Figure 4a. We find the range of solutions with small average elevation misfits ( $\sim 360 \text{ m}$ ) have  $\beta/\alpha \sim 11$ , with a well-defined minimum misfit solution for  $\alpha$  and  $\beta$  of  $\sim 8$  and  $\sim 85$ , respectively, corresponding to lithospheric mantle-crust, and mantle-asthenosphere density contrasts of  $\sim 400$  ( $\alpha = 8.125$ ) and  $\sim 38 \text{ kg m}^{-3}$ , respectively (Figure 4c). Our best fit lithospheric mantle-crust density contrast is similar to the value ( $414 \text{ kg m}^{-3}$ ) used by Becker et al. (2014) in their analysis of topography here. Figure S2a shows a map of elevation anomaly in this region for our minimum solution of  $\alpha$  and  $\beta$ .

Antarctica also has significant variations in bedrock elevation (after ice unloading) and crustal and lithospheric thicknesses (Priestley et al., 2019). Here, there is up to 3 km difference in elevation between the ice-unloaded bedrock of West and East Antarctica (Figure 6a, Bedmap2, Fretwell et al., 2013). Shen et al. (2018) have determined a detailed crustal structure spanning West and East Antarctic from the inversion of ambient noise surface waves, for a region about 4,000 km across with up to 30 km difference in crustal thickness (Figure 7a). The thickness of the conductive lithosphere varies from less than 80 km beneath the Ross Sea to 200 km thick beneath the Gamburtsev Mountains in East Antarctica, with a marked step

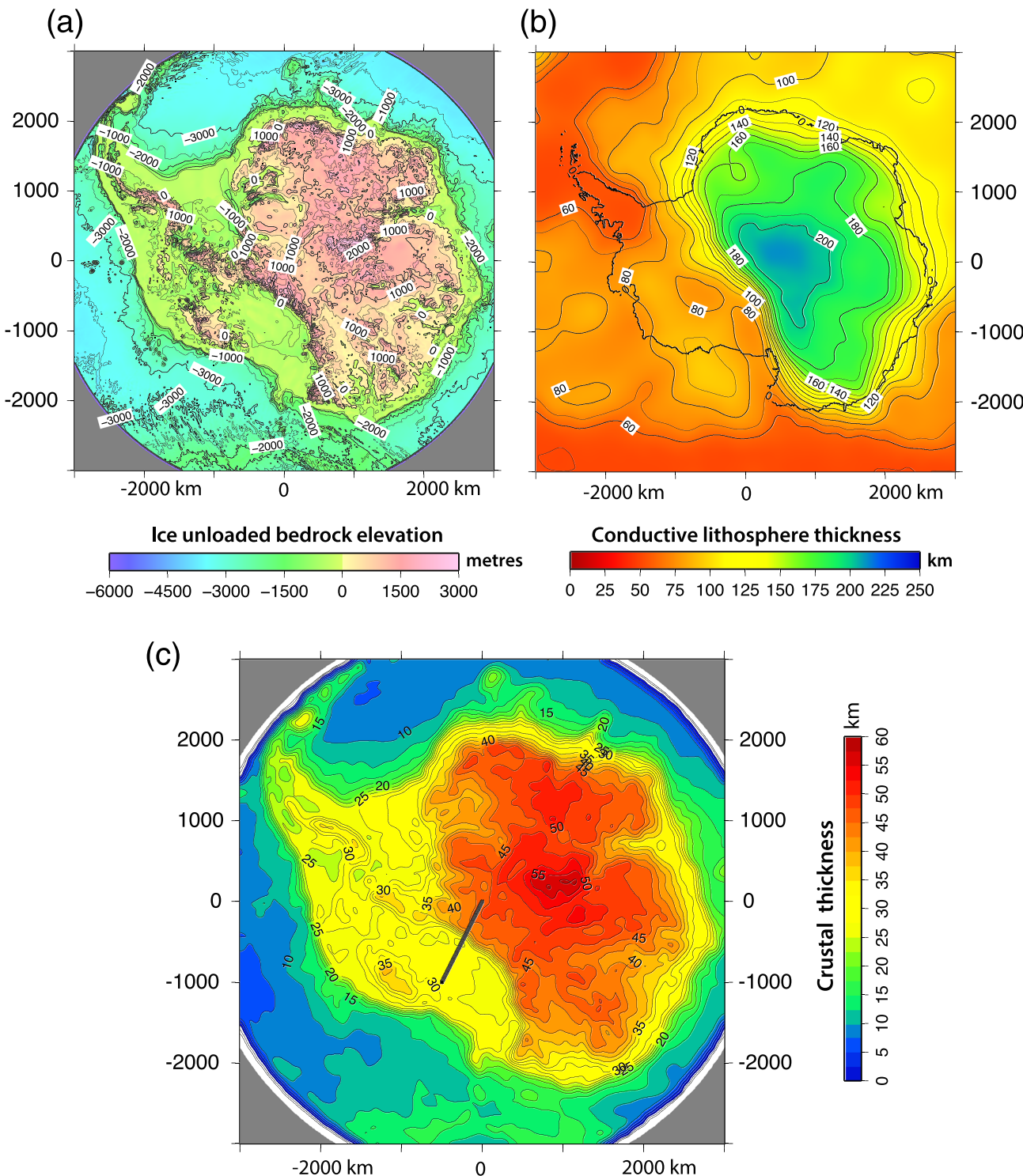


**Figure 6.** Crustal structure of Antarctica calculated from whole lithosphere isostasy (WLI). (a) Bedrock elevations from Bedmap2 (Fretwell et al., 2013), corrected for ice load assuming local isostasy. (b) Conductive lithosphere thickness from Priestley et al. (2019). (c) Crustal thickness derived from WLI (see text) that satisfies both bedrock elevations in (a) and lithospheric thickness in (b), with minimum misfit with crustal model of Shen et al. (2018) for part of Antarctica determined from Rayleigh wave inversion. The crustal model has a reduced chi-square misfit = 0.98 to seismic crustal model, for  $\alpha = 6.5$ ,  $\beta = 65$ , and 32.3 km reference crustal thickness for 100 km thick conductive lithosphere. Thick black line shows profile of gravity model in Figure 7b.

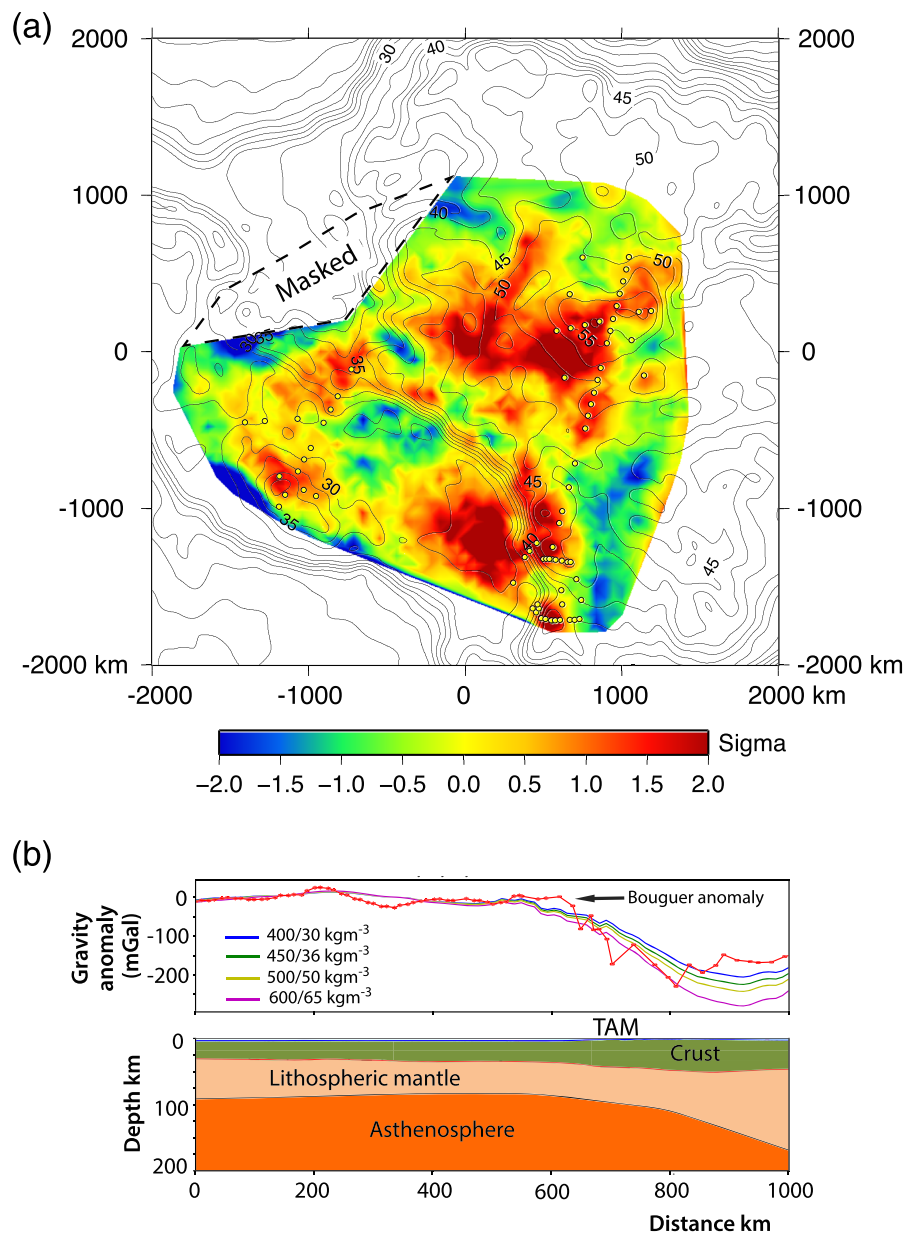


**Figure 7.** (a) Map showing misfit between WLI crustal model (shown as contours) in Figure 6c and Shen et al. (2018) seismic model, expressed in terms of 1 sigma uncertainties in seismic model. Yellow circles show where seismic crustal thickness is constrained by S-wave receiver functions. Masked region in Weddell Sea sector is where WLI misfits >2 sigma, possibly due to poor seismic model resolution or unknown thick sedimentary basins. (b) Observed Bouguer gravity anomalies (points) and model (solid line) based on crustal thickness model and lithospheric structure, along profile in Figure 6c, for indicated density contrasts of lithospheric mantle with crust and asthenosphere, respectively.

beneath the Transantarctic Mountains (Figure 6b; Priestley et al., 2019). In the next section, we use these data in the context of a WLI model of Antarctica to derive values of  $a$  and  $b$ , and corresponding density contrasts for lithospheric mantle with crust and asthenosphere.

## 2. Crustal Structure of Antarctica

Previous models of crustal thickness in Antarctica, based on gravity and receiver function data, placed East Antarctica as a clear outlier compared to the other continents, with an intermediate average crustal

thickness 35–40 km but the highest average bedrock elevation of about 1,000 m after correcting for ice mass loading (Figure 6a). This has prompted a range of explanations including the presence of mantle plumes, hot lines, or anomalous crustal and mantle lithologies beneath East Antarctica (O'Donnell & Nyblade, 2014; Smith & Drewry, 1984). However, determining crustal thickness with  $P$ -wave receiver functions in ice-covered areas has been problematic (Hansen et al., 2009). Moreover, because much of Antarctica is covered in ice up to 4 km thick, with an extreme climate, it has not been possible to use seismic refraction and reflection crustal profiling methods deployed in most continents. Receiver function estimates have been limited to continent-scale traverses, with more detailed studies in the vicinity of the Transantarctic Mountains. Regional gravity inversion estimates are inherently nonunique, requiring an assumption about the average thickness of the crust as well as crustal densities, and this modeling generally ignores the contribution of variation in thickness of the lithospheric mantle to the gravity field (Block et al., 2009; O'Donnell & Nyblade, 2014). However, crustal structure derived from inversion of Rayleigh surface wave data and  $S$ -wave receiver functions are largely independent of the drawbacks of previous attempts to measure crustal thickness (Shen et al., 2018).

## 2.1. Data and Methodology for Constructing Crustal Model of Antarctica

We use the Bedmap2 compilation of data for Antarctica (Fretwell et al., 2013, <https://www.the-cryosphere.net/7/375/2013/>). We grid these data at 5 km spacing, using a stereographic projection, of the ice thickness and elevation of the bedrock in a region extending from the South Pole to 60°S. We calculate the crustal model in the following steps:

1. The ice load is calculated by smoothing with a Gaussian filter, using GRDFILTER in GMT (Wessel et al., 2013). The choice of smoothing is arbitrary and depends on the appropriate elastic thickness—we use a 3 sigma radius of 120 km for the filter, which is a compromise between local WLI and some flexural rigidity. Sensitivity tests show that the choice of smoothing parameters has a negligible effect on the final crustal model.
2. The effect of the ice load on bedrock elevation is calculated at each grid point by assuming local isostasy, using the thickness of the smoothed ice sheet ( $h_{\text{ice}}$ ) calculated above, and adding the simple correction  $(\rho_{\text{ice}}/\rho_a) h_{\text{ice}}$  to the observed bedrock elevation, where  $\rho_{\text{ice}}$  and  $\rho_a$  are the ice and asthenospheric densities, respectively. Note that the water load is corrected in a similar way. We then smooth the backstripped bedrock elevations in the same way as the ice load (i.e., Gaussian filter with 3 sigma radius = 120 km)—this approximates a moving window average with a box width of 100 km, equivalent to our original lithosphere gridding.
3. The lithospheric thickness at each grid point is calculated from an interpolation of the Priestley et al. (2019) 1° gridded lithosphere thickness (Figure 6b).
4. The crustal thickness (Figure 6c) is then calculated using Equation 2 from the local ice-unloaded elevations determined in (2). We then search for a minimum misfit, given the quoted uncertainties in the crustal model (expressed as reduced chi-square parameter), between the observed crustal thickness from Shen et al. (2018) and our WLI model, sampling the data and observations at 50 km intervals. This is achieved by iterating on three parameters defining the crustal thickness at sea level for a 100 km thick conductive lid, and  $\alpha$  and  $\beta$  in Equation 2.

## 2.2. Best Fit Antarctic WLI Crustal Model (Data Set S1)

We found solution sets to our WLI crustal model for Antarctica that fit the seismically determined crustal structure of Shen et al. (2018) virtually everywhere with the quoted 1.5 sigma uncertainties. However, we found that the fits are always outside the quoted 2 sigma uncertainties in the Weddell Sea sector, comprising about 12% of the total area of seismic model (Figure 7a). The reasons for this are unclear but may be a consequence of poor resolution in the lithospheric and bedrock models, the presence of unexplored thick and lower density sedimentary basins beneath the Weddell Sea, and possible systematic errors in the seismic model where there is no receiver function data. We mask out this small area, in order not to bias the rest of our best fitting WLI models in the remaining 88% of the region (Figure 7a).

We find that we can constrain upper bounds of  $\sim 8$  for  $\alpha$  and  $\sim 110$  for  $\beta$ , for models that fit on average the observations of crustal thickness with a reduced chi-square  $< 1.035$  with a  $p$  value  $> 10\%$  that the data fit the model for the number of observations  $n = 2,644$  (Figures 6c and 7a). However, we find that there is a

strong trade-off between  $\alpha$  and  $\beta$ , but  $\beta/\alpha$  is in the range 10 to 14. Our best fit value of the crustal thickness for 100 km thick conductive lithosphere is 32.3, essentially identically to that determined from our global compilation of crustal and conductive lithosphere thicknesses for elevations within 50 m of sea level (Figure 4a). Assuming a reference asthenospheric density of  $3,250 \text{ kg m}^{-3}$ , our WLI analysis of Antarctica constrains density contrasts for conductive lithosphere mantle with crust, and with asthenosphere, of  $>400$  and  $>30 \text{ kg m}^{-3}$ , respectively. We additionally constructed a forward Bouguer gravity model, based on the free air gravity anomalies from Scheinert et al. (2016), across the lithospheric step beneath the Transantarctic Mountains (Figure 6c). We found that the model reproduced the amplitude and shape of the observed gravity anomaly for a lithospheric mantle-crust density contrast of 400 to 500  $\text{kg m}^{-3}$  and a conductive lithosphere-asthenosphere density contrast of 30 to 50  $\text{kg m}^{-3}$  (Figure 7b).

The excellent fit over such wide crustal and lithospheric ranges in thickness ( $\sim 30$  and  $\sim 200$  km, respectively) to the observed crustal thicknesses, for density contrasts of lithospheric mantle with crust and asthenosphere that are typical of those derived from studies in other continents, discussed above, supports the conclusion that there is nothing anomalous about the lithospheric mantle beneath Antarctica, contrary to the previous suggestions (O'Donnell & Nyblade, 2014). The WLI crustal model also provides a simple explanation for the relatively high average elevation of East Antarctica (1,020 m above sea level, after the effects of ice load are removed) in terms of the relatively thick crust, with an average thickness of about 45 km, compared to 38–42 km for the other continental interiors (Figure 3b, North America, South America, Africa, Australia, Eurasia, and India), given these continents have similar average lithospheric thicknesses (170–190 km). Finally, the model suggests that the Antarctic lithosphere approximates local isostasy at the hundreds to thousands of kilometers scale. We investigate these ideas further in the following sections.

Figure 6c shows an excellent fit crustal model of Antarctica (reduced chi-square = 0.98,  $p$  value  $>50\%$ ), based on the analysis described above, for  $\alpha = 6.5$  and  $\beta = 65$ , and 32.3 km thick crust at sea level for 100 km thick conductive lithosphere (Data Set S1). For completeness, we also assign a value of 6.5 for  $\alpha$  and 65 for  $\beta$  where the crustal model extends to elevations  $<-1,700$  m, in order to fit the typical thickness of oceanic crust.

### 3. WLI and Average Elevations of Continental Interiors (Data Set S2)

Both average crustal and average conductive lithospheric thickness will vary from continent to continent, and so we isolate the crustal effect by calculating from Equation 2 what the elevation would be for a conductive lithosphere with a specified standard thickness (see further on), given its actual crustal and conductive lithospheric thickness. This elevation is referred to as the reduced elevation ( $h_{\text{reduced}}$ ):

$$h_{\text{reduced}} = h_{\text{observed}} + (L_{\text{observed}} - L_{\text{standard}})/\beta, \quad (3)$$

where  $\beta$  is defined as before (Equation 2) and  $L_{\text{observed}}$  is the observed lithospheric thickness and  $L_{\text{standard}}$  the lithospheric thickness that is being used to standardize elevations. For the actual lithospheric thickness, we use the Priestley et al. (2019) global conductive lithospheric thickness map, and we choose a standard reference conductive lithosphere thickness  $L_{\text{standard}}$  of 100 km.

We adopt a value for  $\beta$  of 93, equivalent to a conduction lithosphere-asthenosphere density contrast of  $35 \text{ kg m}^{-3}$  for a reference asthenospheric density of  $3,250 \text{ kg m}^{-3}$ . This is typical of the range indicated by best fit solutions in western North America, Antarctica, and gravity studies in New Zealand, discussed in sections 1.2 and 2.2. Figure 3c (Data Set S2) shows a plot of average crustal thickness against reduced elevation (corrected for water load where appropriate), as defined by Equation 3, both for  $1 \times 1^\circ$  grid squares and whole continental interiors averaged over thousands of kilometers (Figure 3a), using this value of  $\beta$ . Plotting the data this way, we have effectively isolated the role of crustal thickness in controlling elevation; note that the choice of standard lithosphere does *not* affect the slope of the plot. It is clear that for the averaged continental interiors this now reveals the linear relation that would be predicted by Airy isostasy, with  $R^2$  fit of 0.943.

For all the continents in Figure 3c, there is no information about the density difference between mantle and crust was used, either for crustal thickness or reduced elevations; the slope of the plot provides an independent estimate of this. For the best fitting linear trend of the averaged continental interiors, the slope is  $1/\alpha$ , where  $\alpha = 7.8$ . This implies a ratio  $\beta/\alpha \sim 12$ , or a conductive lithosphere mantle-crust density contrast of

$417 \text{ kg m}^{-3}$ , for a reference asthenospheric density of  $3,250 \text{ kg m}^{-3}$ . Again, these values are typical of those derived from gravity and regional analyses of WLI described previously (see sections 1.2 and 2.2). Thus, WLI applied to all the continents not only makes sense of the variation in average elevation of continental interiors but also shows that the average density contrasts for the continental crust, conductive lithosphere, and asthenospheric parts of the underlying mantle are globally consistent.

WLI requires the conductive lithospheric mantle in the continents to be on average more dense than the underlying asthenospheric mantle, and so continental roots are generally negatively buoyant and do not need to be “dragged” down in convective downwellings but have the potential to sink on their own. Thus, although mantle depletion in the continental lithosphere due to melt extraction and other processes may lead to lower density for any given temperature, the effect of the coefficient of expansion must win out overall—our analysis of WLI suggests that a net contrast of  $30\text{--}40 \text{ kg m}^{-3}$  is a good estimate on continent-wide scales, although this might vary outside this range on more local scales. Assuming an undepleted density contrast  $\sim 50 \text{ kg m}^{-3}$ , this indicates  $10\text{--}20 \text{ kg m}^{-3}$  average depletion (Crosby et al., 2010).

#### 4. Factors Controlling Deviations From Global WLI Model (Data Sets S3–S7)

We now derive a reference global map of elevation anomalies (Figure 8 and Data Set S3) from Equation 2. This is calculated using the following parameters: (1) for elevations  $>-1,000 \text{ m}$   $\alpha$  and  $\beta$  (7.8 and 93, respectively), defined by the plot of average elevation of continents against average crustal thickness (Figure 3c); (2) for oceanic regions with elevations  $<-1,000$ —note that these regions are not the focus of this study—we use an ad hoc best fit model where  $\alpha$  and  $\beta$  are 6.5 and 65, respectively; (3) a 32 km reference crustal thickness for 100 km thick conductive lithosphere, defined by the plot of crustal thickness against conductive lithospheric thickness for elevations within 50 m of sea level (Figure 4a); (4) crustal thickness and elevations are those in the CRUST 1.0 and Etopo5 databases; and (5) conductive lithosphere thicknesses are those from Priestley et al. (2019). We define an elevation anomaly as the difference between the observed elevation and that for the WLI reference model.

Figure 8 shows that much of the continents have elevations anomalies  $<500 \text{ m}$ . Elevation anomalies in our map could be a consequence of a number of factors: (i) local variations in crustal densities, (ii) errors in the crustal thickness, (iii) local variations in lithospheric mantle and asthenospheric densities, (iv) errors in the conductive lithospheric thickness, (v) effects of lithospheric flexure, (v) true dynamic topography caused by normal stresses generated by mantle flow, and (vi) postglacial rebound. We show below that the first four factors alone can easily contribute to well over 1 km of elevation anomaly (Figure 9). In addition, the effects of flexure are visible at length scales less than about 400 km, where the continents have  $T_e$  of a few tens of kilometers. For example, the negative elevation anomalies along the southern margin of the Himalayas, or in the Persian Gulf, on the margins of the Zagros Mountains, are most likely a flexural response. The marked negative anomaly over the Baltic region and Finland could be in part due to ongoing postglacial rebound since the Last Glacial Maximum, but this would not be expected to contribute not more than a few hundred meters (Ranalli, 1995). Interestingly, a similar negative elevation anomaly is not seen over Hudson Bay in North America, which is the center of postglacial rebound after melting of the Laurentian Ice Sheet—this suggests that uncertainties in all or some of crustal and lithospheric thicknesses and densities swamp the postglacial signal here.

Typical uncertainties in crustal and conductive lithospheric thicknesses are  $\sim 3$  and 30 km, respectively (Molnar et al., 2015; Priestley et al., 2019; Shen et al., 2018), which for our reference values of  $\alpha$  and  $\beta$  (7.8 and 93, respectively) translate into typical elevation anomalies  $\pm 350 \text{ m}$  for each of these two factors. Plausible variations in crustal density could certainly be up to  $\pm 100 \text{ kg m}^{-3}$ , based on seismic velocity-density calibrations (Barton, 1986; Christensen & Mooney, 1995), which translate into a potential elevation anomaly of  $\pm 1.2 \text{ km}$  for 40 km thick crust, using a reference asthenospheric density of  $3,250 \text{ kg m}^{-3}$ . Likewise, for mantle in the conductive lithosphere, plausible variations in density could be in the range  $\pm 30 \text{ kg m}^{-3}$ , depending on the degree of depletion (Crosby et al., 2010), which translates into a potential elevation anomaly of  $\pm 0.9 \text{ km}$  for 100 km thick conductive lithospheric mantle in continental interiors, although its contribution will be much less for thin lithosphere.

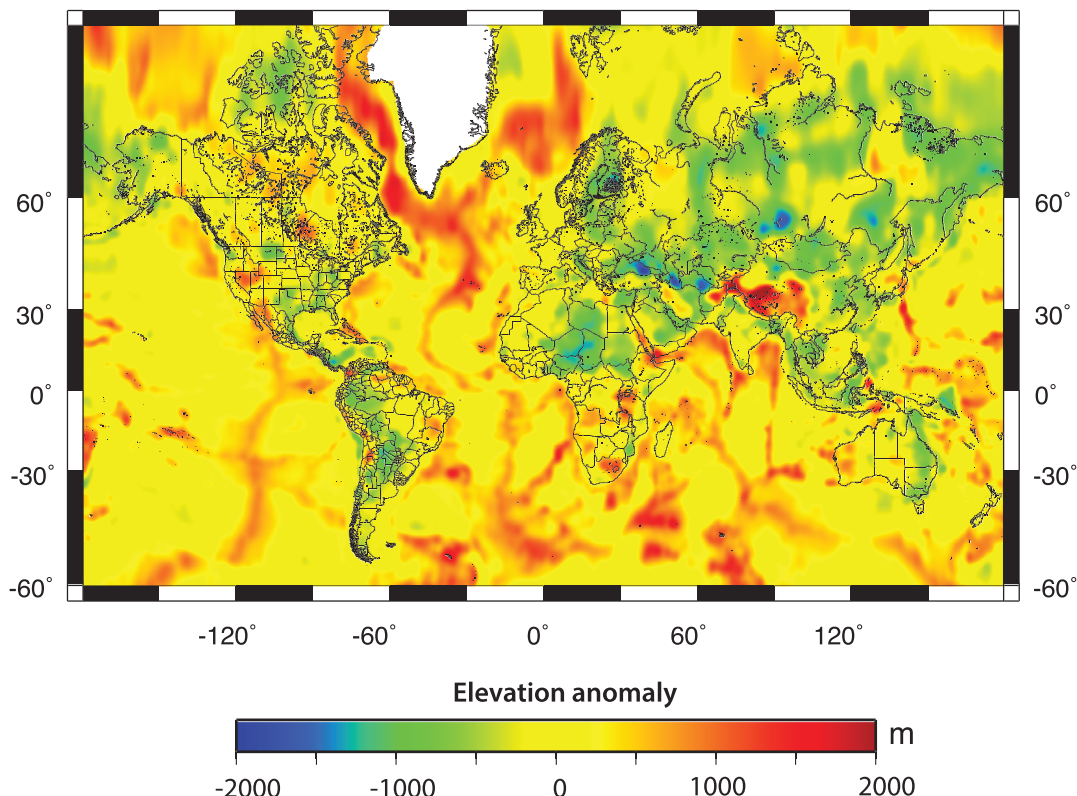


**Figure 8.** Difference between observed elevation and that predicted by whole lithosphere isostasy, using a reference model for the continents (elevations  $>-1,000$  m) for 32 km thick reference crust for 100 km conductive lithosphere derived from Figure 4a, and  $\alpha = 7.8$  and  $\beta = 93$  from Figure 3c. Generally, elevation anomalies  $<500$  m in continental interiors with notable exceptions. In the oceans, a simple model with  $\alpha = 6.5$  and  $\beta = 65$  provides excellent fits, except along the mid-ocean ridges where there is a lack of resolution of the lithospheric thickness determined from surface wave tomography (see text; Priestley et al., 2019). Strong negative elevation anomalies in Africa and South America are most likely a consequence of errors in the crustal model (CRUST 1.0—see text). The reasons for the strong positive anomaly in central Asia in the vicinity of Tibet are controversial but may in part be due to smearing of conductive lithosphere structure here.

The total contribution of uncertainties in crustal and mantle densities and thicknesses to the elevation anomaly depends on how these uncertainties correlate. Assuming that they are uncorrelated, then their total contribution to the elevation anomaly is  $\sim\pm 0.7$  km at the 1 sigma level, but it could be much higher if they are systematically correlated, acting in the same direction and extending over wide areas. For example, studies using different methodologies suggest that CRUST 1.0 may systematically overpredict the thickness of the crust by up to  $\sim 5$  km in significant parts of South America and Africa (Figures 9 and S3; Van der Meijde et al., 2015).

We plot the required perturbation (referred to as anomaly in Figure 9) in crustal and conductive lithosphere mantle thicknesses and densities that individually account for the elevation anomalies in our reference model in Figures 9a–9d (Data Sets S4–S7). It is clear that variations in crustal density up to  $100 \text{ kg m}^{-3}$  can explain virtually all the elevation anomaly in the continents, and in regions of thick conductive lithosphere beneath continental interiors, variations in mantle density up to  $30 \text{ kg m}^{-3}$  can likewise achieve the same effect. Interestingly, Archaean continental cores, such as the Kaapvaal Pilbara cratons in southern Africa and Australia, are consistently associated with small positive elevation anomalies that could be explained by significantly more depleted mantle lithosphere (up to  $30 \text{ kg m}^{-3}$  depletion), whereas slightly negative elevation anomalies in regions of terrane accretion along continental margins (e.g., eastern Australia or parts of the Pacific rim) could be explained by slightly denser continental crust with a greater mafic component (Figures 8, 9a, and S3). Much of Eurasia is also associated with small negative crustal density anomalies (Figures 8 and 9a). Thus, the elevation anomalies appear to correlate, at least locally, with crustal and tectonic provinces.

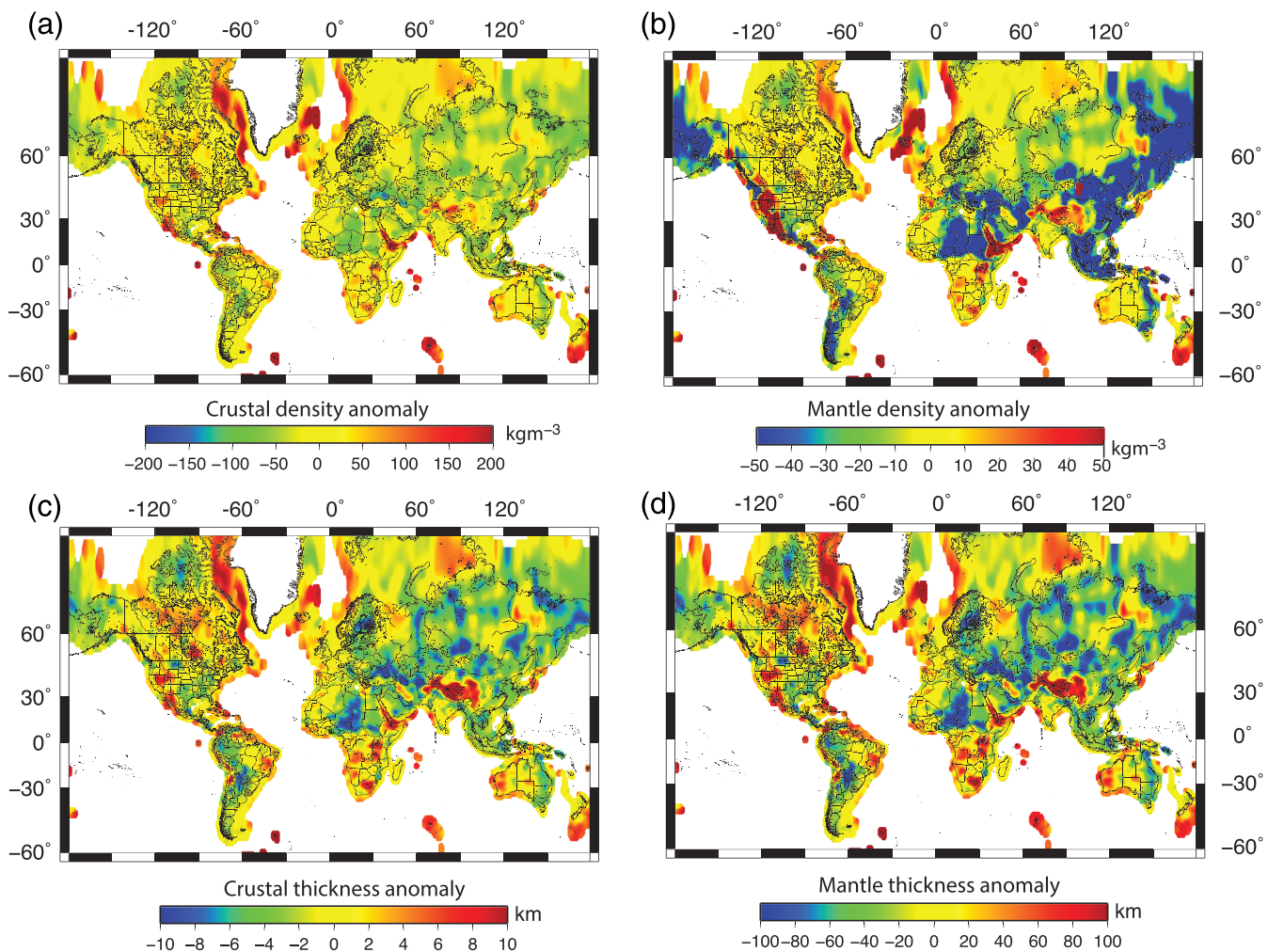


**Figure 9.** Perturbations (referred to as anomalies) in reference continental model required to explain all elevation anomalies in continents. (a) Crustal density perturbations from reference model. Note that almost all elevation anomalies can be explained by a perturbation of average crustal density up to  $100 \text{ kg m}^{-3}$ . (b) Perturbation in conductive lithosphere mantle density. In regions with thick lithosphere ( $>150 \text{ km}$ ), small variations in mantle density up to  $30 \text{ kg m}^{-3}$  can largely account for elevation anomaly. (c) Departures in crustal thickness from CRUST 1.0. This may be an important source of error in Saharan Africa and South America where there are limited crustal data. (d) Departures in conductive lithosphere thickness from Priestley et al. (2019) lithosphere model.

## 5. Discussion

The previous analysis shows that variations in the thickness of the conductive lithosphere have a first-order control on the elevation of the continents, in addition to variations in the thickness of the crust. This way, the concept of a negatively buoyant mantle lithosphere of variable thickness, resting on a lower density asthenosphere, which works so well in the oceans as an explanation for the variation in the depth of the sea floor, is essential to understanding the elevation of the continents, defining WLI. The average density contrasts between conductive lithosphere mantle and crust, as well as with the underlying asthenosphere, appear to show relatively narrow ranges from continent to continent, regardless of the thickness or age of the crust and lithosphere.

### 5.1. Isostasy and Dynamic Topography

WLI provides a consistent framework in which to identify dynamic topography—see also Becker et al. (2014) and Gvirtzman et al. (2016), who adopted a similar approach for an analysis of topography in western North America and the eastern Mediterranean and Persian Gulf region. Here, we follow Molnar et al. (2015) who define dynamic topography as that supported by normal flow stresses in the asthenosphere, as distinct from

the static buoyancy effect of density contrasts—as such, dynamic topography should be apparent in the long wavelength gravity field, giving rise to isostatic gravity anomalies because it will involve vertically uncompensated mass anomalies.

We have shown that a self-consistent conductive lithospheric and crustal model can be derived with zero elevation anomalies, given plausible variations in both crustal and lithospheric densities and uncertainties in thicknesses. As pointed out by Molnar et al. (2015), this indicates that dynamic topography, as defined above, will be hard to identify from WLI unless both crustal and lithospheric densities and thicknesses are accurately known. Plausible uncertainties in WLI parameters could lead to elevation anomalies  $>1$  km and of the order or greater than those typically assumed for dynamic topography (Lithgow-Bertelloni & Silver, 1998). For example, the dynamic effect of the African superswell has been postulated as the cause of the relatively high average elevation ( $\sim 1,000$  m) of Southern Africa (Lithgow-Bertelloni & Silver, 1998; Nyblade & Robinson, 1994), yet, as shown in Figure S3, the topography in southern Africa can easily be accounted for by some combination of plausible variations in the crustal and lithospheric densities, together with uncertainties in their thicknesses, in the context of our simple model of WLI without requiring “dynamic” effects. This conclusion is supported by the small isostatic gravity anomalies in this region (Molnar et al., 2015).

The elevations in West Antarctica have also been related to the dynamic effect of a plume (Sutherland et al., 2010) yet can be explained by simple WLI with surprisingly uniform average crustal and mantle densities (Figures 8 and 9). However, we concur with Becker et al. (2014) that dynamic effects cannot be ruled out as a factor supporting the high elevations in the Basin and Range province of western North America (Figure S2a), although our analysis indicates that its role would be smaller ( $<500$  m) than they suggested. In this respect, we note that crustal density anomalies derived from seismic velocities (Becker et al., 2014; Lowry & Pérez-Gussinyé, 2011) act in the right direction, helping to explain elevations (Figure S2b). The negative elevation anomalies in Europe (Figure S4a) could be explained by locally thicker lithosphere than resolved by Priestley et al. (2019), especially in the zone of convergence in the Adriatic that might be a nascent subduction zone. Likewise, an explanation for the positive elevations in central Spain and the Massif Central in central France could be locally thinner lithosphere than currently resolved.

One source of dynamic topography is the flow field during the creation of a Rayleigh-Taylor instability (Houseman et al., 1981) or Stokes flow due to a falling body in the asthenosphere (Morgan, 1965). During the detachment process static isostasy will not describe the vertical force balance as there will be stresses generated by both crustal and mantle flow. The horizontal length scale of this detachment may be less than the resolution of the lithospheric structure imaged by surface wave tomography ( $\sim 250$  km, Priestley et al., 2019). Thus, the longer wavelength elevation anomalies in WLI shown in Figure 8 are unlikely to be a consequence of dynamic topography due to Rayleigh-Taylor instabilities in the “act,” so to speak.

The longer wavelength lithospheric structure is inherently unstable for low values of  $\beta$  in Equation 2 (i.e., larger conductive lithosphere mantle-asthenosphere density contrasts). But detachment of lithospheric mantle will only initiate if there is a strong lateral perturbation in the thickness of the conductive lithosphere—once this happens, detachment may develop slowly, depending on the viscosity of the mantle (Houseman et al., 1981). It is possible that the Mesozoic and/or Cenozoic uplift history of Southern Africa (Lithgow-Bertelloni & Silver, 1998) may be simply due to episodic thinning of the lithosphere as part of some sort of slow Rayleigh-Taylor instability. In this regard, it is notable that this region has the thinnest average lithosphere ( $\sim 170$  km) of the continental interiors defined in this study.

## 5.2. Lithospheric and Elastic Thickness ( $T_e$ )

The general paucity of earthquakes in the mantle has led some authors to suggest that the continental lithospheric mantle has no elastic strength on both short and long timescales (Jackson et al., 2008; Maggi et al., 2000; McKenzie & Fairhead, 1997). However, Figure 10 shows that there is a striking and broad correlation between the estimates of elastic thickness from gravity and topographic data using the coherence method (Lowry & Pérez-Gussinyé, 2011; Pérez-Gussinyé et al., 2004, 2007, 2008, 2009; Pérez-Gussinyé & Watts, 2005; Swain & Kirby, 2006) and the conductive lithosphere thickness inverted from seismic data (Priestley et al., 2019). Similar conclusions have been reached on the basis of analysis of regional  $T_e$  data from Canada (Hyndman et al., 2009) and various mountain ranges (Lamb & Watts, 2010). Since  $T_e$  is larger

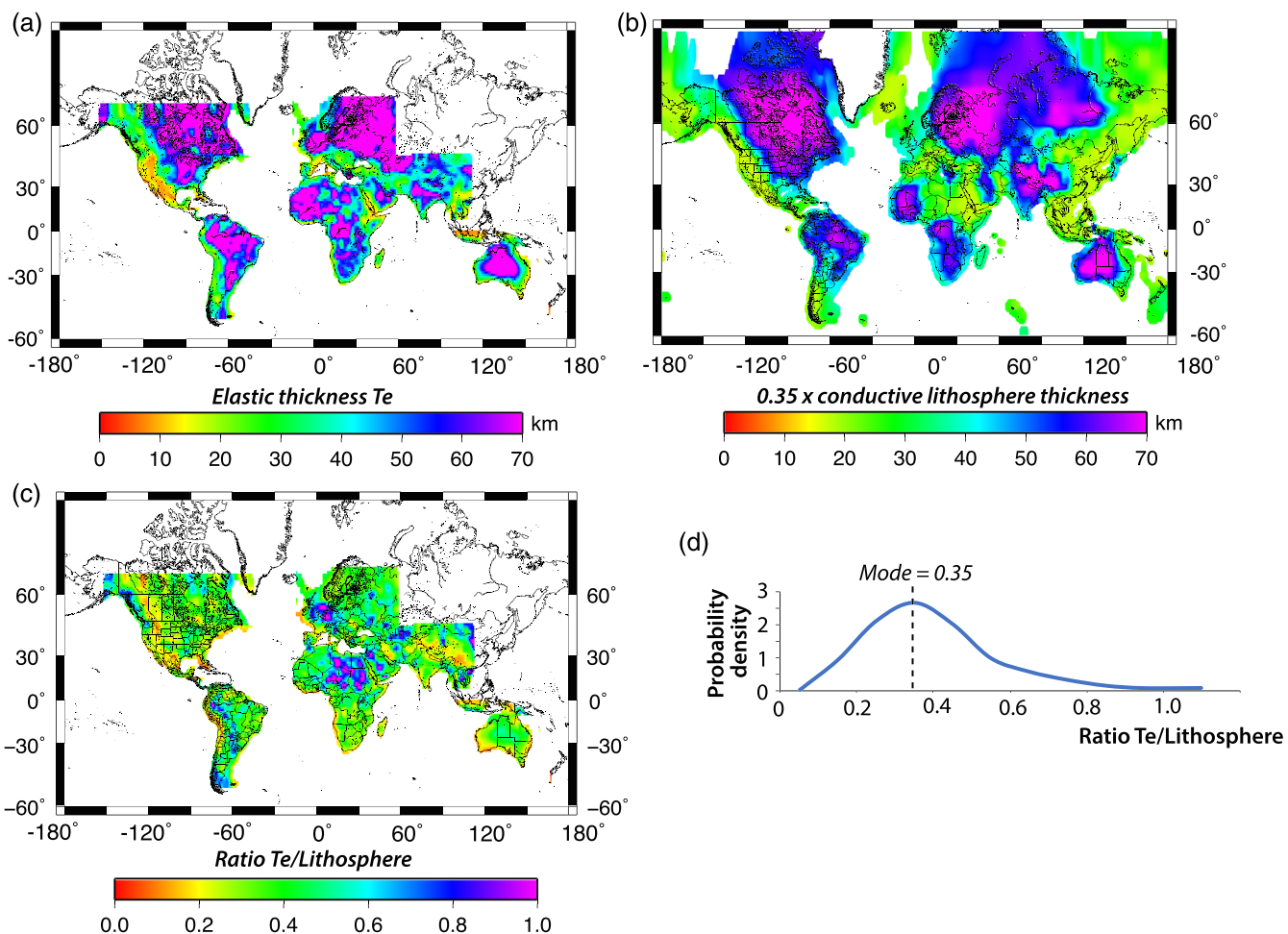


**Figure 10.** Continental elastic thickness  $T_e$ . (a)  $T_e$  estimated from gravity coherence studies—see text. (b) Conductive lithosphere thickness from Priestley et al. (2019), scaled by a factor 0.35 (modal value in d). (c) Ratio of elastic thickness  $T_e$  to conductive lithosphere thickness. (d) Histogram of ratios in (c), given as a probability density function (area under curve = 1). It is clear that ~70% of continents are in the range 0.25 to 0.5, with a mode of ~0.35, indicating that elastic thickness broadly correlates with conductive lithosphere thickness, and the mantle part of the lithosphere plays an important role in long-term lithospheric strength.

than crustal thickness in many areas, this suggests that the mantle also contributes to the elastic strength of the lithosphere. Also, it indicates that the temperature in continental interiors plays a crucial control on lithospheric strength, as has been already suggested by various authors (Burov, 2010, 2011; Burov & Diamant, 1995; Burov & Watts, 2006; Hyndman et al., 2009; Tesauro et al., 2012).

The results in Figure 10 show a large range of elastic thickness ( $T_e$ ) values from around 10 km at active continental rift zones to 70 km or more in cratonic regions ( $T_e$  values from a compilation of published and unpublished  $T_e$  data). These  $T_e$  values have been computed with the coherence method, using wavelets (in Australia, Kirby & Swain, 2006; Swain & Kirby, 2006) and moving windows of  $600 \times 600$  km everywhere else. This window size affords a good lateral resolution but cannot resolve large  $T_e$  values; therefore, we have capped  $T_e$  values at 70 km (Lowry & Pérez-Gussinyé, 2011; Pérez-Gussinyé et al., 2004, 2007, 2008, 2009; Pérez-Gussinyé & Watts, 2005; Swain & Kirby, 2006). Hence, when comparing  $T_e$  and conductive lithosphere thickness it is important to keep in mind that the  $T_e$  estimates shown here cannot resolve differences in  $T_e$  values for large lithospheric thicknesses. On the other hand, the method used by Priestley et al. (2019) cannot resolve conductive lithospheres much thinner than 50 km and has a lateral resolution of 250 km, suggesting that in places where  $T_e$  shows a great deal of variation and detail, as in the East African rift (Pérez-Gussinyé et al., 2009), estimates of the conductive lithosphere thickness may not exhibit such detail.

Watts and Moore (2017) have analyzed the contribution of the gravity due to topography and its flexural compensation on the power spectra of the Earth's gravity field. They find that both the topography and its flexural compensation can explain the power spectra of the Earth's gravity field for wavelengths between 100 and 1,200 km. This is in agreement with the result shown here that topography is compensated at the base of the conductive lithosphere, at large wavelengths (i.e., more than several hundred kilometers). Watts and Moore (2017) found a global average for  $T_e$  of ~34 km, which, taking into account the global average conductive lithospheric thickness estimated here (~97 km), conforms to a general relation of  $T_e \sim 0.35 L$  (Figure 10b). We plot the ratio of  $T_e$  determined from gravity coherence studies (Figure 10) to observed conductive lithospheric thickness (Priestley et al., 2019) for  $1 \times 1^\circ$  grid squares (Figure 10c). This indicates that for ~70% of the continents, this ratio is in the range 0.25–0.5, with a modal value of 0.35 identical to that estimated from global averages (Figure 10d, Watts & Moore, 2017). Departures of the ratio from these values may be related to different lateral resolutions in the conductive lithosphere thickness and  $T_e$  maps and/or problems with the  $T_e$  estimation techniques.

### 5.3. Crustal Thickness and Continental Erosion

Our new crustal model for Antarctica, based on WLI and conforming closely with both seismic estimates and the global trend, indicates that East Antarctica's high elevation is mainly due to crust on average 3–5 km thicker than the other southern continents. Since 250 Ma, when the continents formed Pangea and Gondwana, there is no evidence for major intracontinental shortening or rifting events that could have resulted in significant changes in crustal thickness. We speculate that the subsequent long-term crustal evolution for the continental interiors has been one of slow crustal thinning due to erosion alone, leading to overall subsidence of the interior. Given that the average crustal thickness of most continental interiors is ~40 km (Figures 3a and 3b), this would require the average crustal thickness to be >40 km in the past 250 Myr. We note, however, that southern Africa, with its relatively high average elevation, may have a more complex history of erosion and elevation change (Lithgow-Bertelloni & Silver, 1998; Nyblade & Robinson, 1994).

At breakup of Gondwana, all the southern continents except East Antarctica moved northwards away from the South Pole, whereas Antarctica drifted southwards over the South Pole. We suggest that this tectonic evolution ensured that Antarctica experienced persistent cold climatic conditions near the South Pole over much of the Phanerozoic, leading to significantly reduced erosion rates that preserved a thicker crust compared to the other continents.

## 6. Conclusions

Simple Airy isostasy that only considers a flotational equilibrium between the crust and underlying mantle lithosphere fails to explain the elevations of the continents, leading directly to the so-called Airy "failure" for crustal thickness in the range 25–50 km thick for which average elevations of the continental interiors are only weakly correlated with crustal thickness.

A simple three-layer model of WLI, in which flotational equilibrium occurs at the base of the conductive lithosphere rather than crust, provides an explanation for the elevation of the continents, given plausible variations in density contrast for conductive lithosphere with crust and with asthenosphere, together with observed variations in crustal and conductive lithosphere thickness. Thus, the concept of a negatively buoyant mantle lithosphere is essential to understanding the elevation of the continents both in their interiors and at their edges. We define two parameters,  $\alpha$  and  $\beta$ , which define reciprocals of average density contrasts for lithospheric mantle with crust and asthenosphere, normalized to a reference asthenospheric density. The ratio  $\beta/\alpha$  appears to show very little regional variation from continent to continent and is in the range 10 to 16, associated with typical average density contrasts of 300 to 550 and 20 to 40  $\text{kg m}^{-3}$ , respectively, suggesting moderate average depletion of lithospheric mantle.

We derive a new crustal model for Antarctica, based on WLI, for constant crustal, lithospheric mantle, and asthenospheric densities, and ignoring the effects of lithospheric flexure, but taking into account the thickness of the conductive lithosphere determined from seismic observations (Priestley et al., 2019). For a zero elevation reference lithosphere 100 km thick, with 32.3 km thick crust, and  $\beta/\alpha \sim 11$ , with  $\alpha < 7.2$  and  $\beta < 90$ , our crustal model has excellent fits (reduced chi-square <1.045) to seismic estimates and gravity

observations. This shows that East Antarctica's high elevation, after removing the ice load, is mainly due to crust on average 3–5 km thicker than the other southern continents. We suggest that Antarctica has experienced persistent cold climatic conditions near the South Pole over much of the Phanerozoic, leading to significantly reduced erosion rates that preserve a thicker crust.

We compare average elevations of continental interiors to their average crustal thickness. This shows that if a correction is made for the negative buoyancy of the average conductive lithosphere thickness for each continent (taking a typical conductive lithosphere–asthenosphere density contrast in this study of  $35 \text{ kg m}^{-3}$ ), then the continents show a well-defined linear relation ( $R^2 = 0.943$ ) between elevation and crustal thickness. This reveals the average mantle–crust density contrast for the continents of  $417 \text{ kg m}^{-3}$  ( $\alpha = 7.8$ ).

We construct a global reference model of WLI using the CRUST 1.0 database, together with seismic observations of conductive lithosphere thickness (Priestley et al., 2019). We define an elevation anomaly in terms of the discrepancies between observed and predicted elevations, which can be explained in terms of plausible uncertainties in (i) local variations in crustal densities, (ii) errors in the crustal thickness, (iii) local variations in lithospheric mantle and asthenospheric densities, (iv) errors in the conductive lithospheric thickness, and (v) local effects of lithospheric flexure. This supports the conclusion of Molnar et al. (2015) that dynamic topography due to normal flow stresses in the asthenosphere is less than a few hundred meters, as indicated by the small regional isostatic gravity anomalies.

There is a correlation between conductive lithosphere thickness and elastic thickness ( $T_e$ ) determined from analysis of gravity and topography. For ~70% continents, the ratio of  $T_e$  to conductive lithosphere thickness is in the range 0.25 to 0.5 with a modal value of 0.35. This supports the idea that  $T_e$  is thermally controlled and the mantle part of the lithosphere plays an important role in determining short- and long-term lithospheric strength.

## Data Availability Statement

Data used in this study come from published sources cited in the manuscript or available in data repositories (ETOPO1: <https://www.ngdc.noaa.gov/mgg/global/>; CRUST 1.0: Laske et al., 2013, and <https://igppweb.ucsd.edu/~gabi/crust1.html>; lithospheric structure: Priestley & McKenzie, 2013, and <http://ds.iris.edu/ds/products/emc-cam2016/>; Bedmap2 Antarctic data: Fretwell et al., 2013, and <https://www.the-cryosphere.net/7/375/2013/>; Antarctic gravity data from Scheinert et al., 2016; and elastic thickness is a compilation of data from Swain & Kirby, 2006; Lowry & Perez-Gussinye, 2011; Pérez-Gussinyé et al., 2004, 2007, 2008, 2009; Pérez-Gussinyé & Watts, 2005). Tabulations of outputs in this study are available at [https://zenodo.org/record/4031646#.X2LYtNaxW\\_g](https://zenodo.org/record/4031646#.X2LYtNaxW_g) (<https://doi.org/10.5281/zenodo.4031646>) and are also available in the supporting information as eight data sets.

## Acknowledgments

We would like to thank Keith Priestley and Dan McKenzie for introducing us to their lithospheric models. Tony Watts has been a constant source of inspiration. We are particularly grateful to Claire Currie and Tony Lowry for very helpful and insightful reviews that have greatly improved the manuscript.

## References

- Airy, G. B. (1855). On the computation of the effect of the attraction of mountain-masses, as disturbing the apparent astronomical latitude of stations in geodetic surveys. *Philosophical Transactions of the Royal Society of London*, 145, 101–104. <https://doi.org/10.1098/rstl.1855.0003>
- Airy, G. B. (1856). XIV. Account of pendulum experiments undertaken in the Harton Colliery, for the purpose of determining the mean density of the earth. & XV. Supplement to the “Account of pendulum experiments undertaken in the Harton Colliery”; being an account of experiments undertaken to determine the correction for the temperature of the pendulum. *Philosophical Transactions of the Royal Society of London*, 146, 297–355. <https://doi.org/10.1098/rstl.1856.0015>
- Allen, P. A., & Allen, J. R. (2013). *Basin analysis: Principles and application to petroleum play assessment*. Chichester, England: John Wiley & Sons.
- Barton, P. J. (1986). The relationship between seismic velocity and density in the continental crust—A useful constraint? *Geophysical Journal International*, 87(1), 195–208. <https://doi.org/10.1111/j.1365-246x.1986.tb04553.x>
- Becker, T. W., Faccenna, C., Humphreys, E. D., Lowry, A. R., & Miller, M. S. (2014). Static and dynamic support of western United States topography. *Earth and Planetary Science Letters*, 402, 234–246. <https://doi.org/10.1016/j.epsl.2013.10.012>
- Bird, P., & Baumgardner, J. (1981). Steady propagation of delamination events. *Journal of Geophysical Research*, 86(B6), 4891–4903. <https://doi.org/10.1029/JB086iB06p04891>
- Block, A. E., Bell, R. E., & Studinger, M. (2009). Antarctic crustal thickness from satellite gravity: Implications for the Transantarctic and Gamburtsev Subglacial Mountains. *Earth and Planetary Science Letters*, 288(1–2), 194–203. <https://doi.org/10.1016/j.epsl.2009.09.022>
- Bourguignon, S., Savage, M. K., & Stern, T. (2007). Crustal thickness and Pn anisotropy beneath the Southern Alps oblique collision, New Zealand. In *Geophysical structure of the Southern Alps Orogen, South Island, New Zealand, Geophysical Monograph Series* (Vol. 175, pp. 115–122). Washington, DC: American Geophysical Union. <https://doi.org/10.1029/175GM12>

- Burov, E. B. (2010). The equivalent elastic thickness ( $T_e$ ), seismicity and the long-term rheology of continental lithosphere: Time to burn-out “crème brûlée”? Insights from large-scale geodynamic modeling. *Tectonophysics*, 484(1–4), 4–26. <https://doi.org/10.1016/j.tecto.2009.06.013>
- Burov, E. B. (2011). Rheology and strength of the lithosphere. *Marine and Petroleum Geology*, 28(8), 1402–1443. <https://doi.org/10.1016/j.marpetgeo.2011.05.008>
- Burov, E. B., & Diamant, M. (1995). The effective elastic thickness ( $T_e$ ) of continental lithosphere: What does it really mean? *Journal of Geophysical Research*, 100(B3), 3905–3927. <https://doi.org/10.1029/94JB02770>
- Burov, E. B., & Watts, A. B. (2006). The long-term strength of continental lithosphere: “Jelly sandwich” or “crème brûlée”? *GSA Today*, 16(1), 4. [https://doi.org/10.1130/1052-5173\(2006\)016<4:tltsoc>2.0.co;2](https://doi.org/10.1130/1052-5173(2006)016<4:tltsoc>2.0.co;2)
- Chapman, D. S., & Pollack, H. N. (1977). Regional geotherms and lithospheric thickness. *Geology*, 5(5), 265–268. [https://doi.org/10.1130/0091-7613\(1977\)5<265:RGALT>2.0.CO;2](https://doi.org/10.1130/0091-7613(1977)5<265:RGALT>2.0.CO;2)
- Christensen, N. I., & Mooney, W. D. (1995). Seismic velocity structure and composition of the continental crust: A global view. *Journal of Geophysical Research*, 100(B6), 9761–9788. <https://doi.org/10.1029/95JB00259>
- Crosby, A. G., Fishwick, S., & White, N. (2010). Structure and evolution of the intracratonic Congo Basin. *Geochemistry, Geophysics, Geosystems*, 11, Q06010. <https://doi.org/10.1029/2009GC003014>
- Dimech, J. L., Stern, T., & Lamb, S. (2017). Mantle earthquakes, crustal structure, and gravitational instability beneath western North Island, New Zealand. *Geology*, 45(2), 155–158. <https://doi.org/10.1130/G38476.1>
- England, P., & Houseman, G. (1986). Finite strain calculations of continental deformation: 2. Comparison with the India-Asia collision zone. *Journal of Geophysical Research*, 91(B3), 3664–3676. <https://doi.org/10.1029/JB091iB03p03664>
- England, P., & Houseman, G. (1989). Extension during continental convergence, with application to the Tibetan Plateau. *Journal of Geophysical Research*, 94(B12), 17,561–17,579. <https://doi.org/10.1029/JB094iB12p17561>
- ETOPO1 (2011). Global 1 arc-minute ocean depth and land elevation from the US National Geophysical Data Center/NESDIS/NOAA/U.S. Department of Commerce. <https://doi.org/10.5065/D69Z92Z5>
- Fischer, K. M., Ford, H. A., Abt, D. L., & Rychert, C. A. (2010). The lithosphere-asthenosphere boundary. *Annual Review of Earth and Planetary Sciences*, 38(1), 551–575. <https://doi.org/10.1146/annurev-earth-040809-152438>
- Fretwell, P., Pritchard, H. D., Vaughan, D. G., Bamber, J. L., Barrand, N. E., Bell, R., et al. (2013). Bedmap2: Improved ice bed, surface and thickness datasets for Antarctica.
- Gvirtzman, Z., Faccenna, C., & Becker, T. W. (2016). Isostasy, flexure, and dynamic topography. *Tectonophysics*, 683, 255–271. <https://doi.org/10.1016/j.tecto.2016.05.041>
- Hansen, S. E., Julia, J., Nyblade, A. A., Pyle, M. L., Wiens, D. A., & Anandakrishnan, S. (2009). Using S wave receiver functions to estimate crustal structure beneath ice sheets: An application to the Transantarctic Mountains and East Antarctic craton. *Geochemistry, Geophysics, Geosystems*, 10, Q08014. <https://doi.org/10.1029/2009GC002576>
- Hasterok, D., & Chapman, D. S. (2007a). Continental thermal isostasy: 1. Methods and sensitivity. *Journal of Geophysical Research*, 112, B06414. <https://doi.org/10.1029/2006JB004663>
- Hasterok, D., & Chapman, D. S. (2007b). Continental thermal isostasy: 2. Application to North America. *Journal of Geophysical Research*, 112, B06415. <https://doi.org/10.1029/2006JB004664>
- Houseman, G., & England, P. (1986). A dynamical model of lithosphere extension and sedimentary basin formation. *Journal of Geophysical Research*, 91(B1), 719–729. <https://doi.org/10.1029/JB091iB01p00719>
- Houseman, G. A., McKenzie, D. P., & Molnar, P. (1981). Convective instability of a thickened boundary layer and its relevance for the thermal evolution of continental convergent belts. *Journal of Geophysical Research*, 86(B7), 6115–6132. <https://doi.org/10.1029/JB086iB07p06115>
- Houseman, G. A., & Molnar, P. (1997). Gravitational (Rayleigh-Taylor) instability of a layer with non-linear viscosity and convective thinning of continental lithosphere. *Geophysical Journal International*, 128(1), 125–150. <https://doi.org/10.1111/j.1365-246X.1997.tb04075.x>
- Hyndman, R. D., & Currie, C. A. (2011). Why is the North America Cordillera high? Hot backarcs, thermal isostasy, and mountain belts. *Geology*, 39(8), 783–786. <https://doi.org/10.1130/G31998.1>
- Hyndman, R. D., Currie, C. A., Mazzotti, S., & Frederiksen, A. (2009). Temperature control of continental lithosphere elastic thickness,  $T_e$  vs.  $V_s$ . *Earth and Planetary Science Letters*, 277(3–4), 539–548. <https://doi.org/10.1016/j.epsl.2008.11.023>
- Jackson, J., McKenzie, D. A. N., Priestley, K., & Emmerson, B. (2008). New views on the structure and rheology of the lithosphere. *Journal of the Geological Society*, 165(2), 453–465. <https://doi.org/10.1144/0016-76492007-109>
- Jordan, T. H. (1975). The continental tectosphere. *Reviews of Geophysics and Space Physics*, 13(3), 1–12. <https://doi.org/10.1029/RG013i003p00001>
- Jordan, T. H. (1978). Composition and development of the continental tectosphere. *Nature*, 275, 745–750. <https://doi.org/10.1038/274544a0>
- Jordan, T. H. (1988). Structure and formation of the continental tectosphere. *Journal of Petrology*, Special Lithosphere Issue, Special Volume, 1, 11–37. [https://doi.org/10.1093/petrology/special\\_volume.1.11](https://doi.org/10.1093/petrology/special_volume.1.11)
- Kind, R., Yuan, X., & Kumar, P. (2012). Seismic receiver functions and the lithosphere-asthenosphere boundary. *Tectonophysics*, 536, 25–43. <https://doi.org/10.1016/j.tecto.2012.03.005>
- Kirby, J. F., & Swain, C. J. (2006). Mapping the mechanical anisotropy of the lithosphere using a 2D wavelet coherence, and its application to Australia. *Physics of the Earth and Planetary Interiors*, 158(2–4), 122–138. <https://doi.org/10.1016/j.pepi.2006.03.022>
- Lamb, S., Smith, E., Stern, T., & Warren-Smith, E. (2015). Continent scale strike-slip on a low-angle fault beneath New Zealand’s Southern Alps: Implications for crustal thickening in oblique collision zones. *Geochemistry, Geophysics, Geosystems*, 16, 3076–3096. <https://doi.org/10.1002/2015GC005990>
- Lamb, S., & Watts, A. B. (2010). The origin of mountains: Implications for the behaviour of Earth’s lithosphere. *Current Science*, 99(12), 1699–1718.
- Laske, G., Masters, G., Ma, Z., & Pasyanos, M. (2013). Update on CRUST1.0—A 1-degree global model of Earth’s crust. In *Geophysical Research Abstracts* (Abstract EGU2013–2658) (Vol. 15, p. 2658). Vienna, Austria: EGU General Assembly.
- Levander, A., & Miller, M. S. (2012). Evolutionary aspects of lithosphere discontinuity structure in the western U.S. *Geochemistry, Geophysics, Geosystems*, 13, Q0AA07. <https://doi.org/10.1029/2012GC004056>
- Lithgow-Bertelloni, C., & Silver, P. G. (1998). Dynamic topography, plate driving forces and the African superswell. *Nature*, 395(6699), 269. <https://doi.org/10.1038/26212>
- Lowry, A. R., & Pérez-Gussinyé, M. (2011). The role of crustal quartz in controlling Cordilleran deformation. *Nature*, 471(7338), 353–357. <https://doi.org/10.1038/nature09912>

- Ludwig, J. W., Nafe, J. E., & Drake, C. L. (1970). Seismic refraction. In A. E. Maxwell (Ed.), *The sea* (Vol. 4, pp. 53–84). New York: Wiley.
- Maggi, A., Jackson, J. A., McKenzie, D., & Priestley, K. (2000). Earthquake focal depths, effective elastic thickness, and the strength of the continental lithosphere. *Geology*, 28(6), 495–498. [https://doi.org/10.1130/0091-7613\(2000\)28%3C495:EFDEET%3E2.0.CO;2](https://doi.org/10.1130/0091-7613(2000)28%3C495:EFDEET%3E2.0.CO;2)
- McKenzie, D. (1978). Some remarks on the development of sedimentary basins. *Earth and Planetary Science Letters*, 40(1), 25–32.
- McKenzie, D. (1989). Some remarks on the movement of small melt fractions in the mantle. *Earth and Planetary Science Letters*, 95(1–2), 53–72. [https://doi.org/10.1016/0012-821X\(89\)90167-2](https://doi.org/10.1016/0012-821X(89)90167-2)
- McKenzie, D., Daly, M. C., & Priestley, K. (2015). The lithospheric structure of Pangea. *Geology*, 43(9), 783–786. <https://doi.org/10.1130/G36819.1>
- McKenzie, D., & Fairhead, D. (1997). Estimates of the effective elastic thickness of the continental lithosphere from Bouguer and free air gravity anomalies. *Journal of Geophysical Research*, 102(B12), 27,523–27,552. <https://doi.org/10.1029/97JB02481>
- McKenzie, D., Jackson, J., & Priestley, K. (2005). Thermal structure of oceanic and continental lithosphere. *Earth and Planetary Science Letters*, 233(3–4), 337–349. <https://doi.org/10.1016/j.epsl.2005.02.005>
- Molnar, P., England, P., & Martinod, J. (1993). Mantle dynamics, uplift of the Tibetan Plateau, and the Indian monsoon. *Reviews of Geophysics*, 31(4), 357–396. <https://doi.org/10.1029/93RG02030>
- Molnar, P., England, P. C., & Jones, C. H. (2015). Mantle dynamics, isostasy, and the support of high terrain. *Journal of Geophysical Research: Solid Earth*, 120, 1932–1957. <https://doi.org/10.1002/2014JB011724>
- Morgan, W. J. (1965). Gravity anomalies and convection currents: 1. A sphere and cylinder sinking beneath the surface of a viscous fluid. *Journal of Geophysical Research*, 70(24), 6175–6187. <https://doi.org/10.1029/JZ070i024p06175>
- Naliboff, J. B., Lithgow-Bertelloni, C., Ruff, L. J., & de Koker, N. (2012). The effects of lithospheric thickness and density structure on Earth's stress field. *Geophysical Journal International*, 188(1), 1–17. <https://doi.org/10.1111/j.1365-246X.2011.05248.x>
- Nyblade, A. A., & Robinson, S. W. (1994). The African superswell. *Geophysical Research Letters*, 21(9), 765–768. <https://doi.org/10.1029/94GL00631>
- O'Donnell, J. P., & Nyblade, A. A. (2014). Antarctica's hypsometry and crustal thickness: Implications for the origin of anomalous topography in East Antarctica. *Earth and Planetary Science Letters*, 388, 143–155. <https://doi.org/10.1016/j.epsl.2013.11.051>
- Parsons, B., & McKenzie, D. (1978). Mantle convection and the thermal structure of the plates. *Journal of Geophysical Research*, 83(B9), 4485–4496. <https://doi.org/10.1029/JB083iB09p04485>
- Parsons, B., & Sclater, J. G. (1977). An analysis of the variation of ocean floor bathymetry and heat flow with age. *Journal of Geophysical Research*, 82(5), 803–827. <https://doi.org/10.1029/JB082i005p00803>
- Pasyanos, M. E., & Nyblade, A. A. (2007). A top to bottom lithospheric study of Africa and Arabia. *Tectonophysics*, 444(1–4), 27–44. <https://doi.org/10.1016/j.tecto.2007.07.008>
- Pérez-Gussinyé, M., Lowry, A. R., Phipps Morgan, J., & Tassara, A. (2008). Effective elastic thickness variations along the Andean margin and their relationship to subduction geometry. *Geochemistry, Geophysics, Geosystems*, 9, Q02003. <https://doi.org/10.1029/2007GC001786>
- Pérez-Gussinyé, M., Lowry, A. R., & Watts, A. B. (2007). Effective elastic thickness of South America and its implications for intracontinental deformation. *Geochemistry, Geophysics, Geosystems*, 8, Q05009. <https://doi.org/10.1029/2006GC001511>
- Pérez-Gussinyé, M., Lowry, A. R., Watts, A. B., & Velicogna, I. (2004). On the recovery of effective elastic thickness using spectral methods: Examples from synthetic data and from the Fennoscandian Shield. *Journal of Geophysical Research*, 109, B10409. <https://doi.org/10.1029/2003JB002788>
- Pérez-Gussinyé, M., Metois, M., Fernández, M., Vergés, J., Fullea, J., & Lowry, A. R. (2009). Effective elastic thickness of Africa and its relationship to other proxies for lithospheric structure and surface tectonics. *Earth and Planetary Science Letters*, 287(1–2), 152–167. <https://doi.org/10.1016/j.epsl.2009.08.004>
- Pérez-Gussinyé, M., & Watts, A. B. (2005). The long-term strength of Europe and its implications for plate-forming processes. *Nature*, 436(7049), 381. <https://doi.org/10.1038/nature03854>
- Platt, J., & England, P. (1994). Convective removal of lithosphere beneath mountain belts—Thermal and mechanical consequences. *American Journal of Science*, 294(3), 307–336. <https://doi.org/10.2475/ajs.294.3.307>
- Pollack, H. N., & Chapman, D. S. (1977). On the regional variation of heat flow, geotherms, and lithospheric thickness. *Tectonophysics*, 38(3–4), 279–296. [https://doi.org/10.1016/0040-1951\(77\)90215-3](https://doi.org/10.1016/0040-1951(77)90215-3)
- Priestley, K., & McKenzie, D. (2006). The thermal structure of the lithosphere from shear wave velocities. *Earth and Planetary Science Letters*, 244(1–2), 285–301. <https://doi.org/10.1016/j.epsl.2006.01.008>
- Priestley, K., & McKenzie, D. (2013). The relationship between shear wave velocity, temperature, attenuation and viscosity in the shallow part of the mantle. *Earth and Planetary Science Letters*, 381, 78–91. <https://doi.org/10.1016/j.epsl.2013.08.022>
- Priestley, K., McKenzie, D., & Ho, T. (2019). A lithosphere-asthenosphere boundary—A global model derived from multimode surface-wave tomography and petrology. In H. Yuan & B. Romanowicz (Eds.), *Lithospheric discontinuities*. <https://doi.org/10.1002/9781119249740.ch6>
- Ranalli, G. (1995). *Rheology of the Earth* (2nd ed.). London: Chapman & Hall.
- Scheinert, M., Ferraccioli, F., Schwabe, J., Bell, R., Studinger, M., Damaske, D., et al. (2016). New Antarctic gravity anomaly grid for enhanced geodetic and geophysical studies in Antarctica. *Geophysical Research Letters*, 43, 600–610. <https://doi.org/10.1002/2015GL067439>
- Scherwath, M., Stern, T., Davey, F., & Davies, R. (2006). Three-dimensional lithospheric deformation under oblique continental collision from gravity analysis in South Island New Zealand. *Geophysical Journal International*, 167(2), 906–916. <https://doi.org/10.1111/j.1365-246X.2006.03085.x>
- Seward, A. M. (2008). *Modelling Pn wave speeds beneath the Central North Island, New Zealand* (Unpublished PhD thesis). Wellington, New Zealand: Victoria University of Wellington.
- Shen, W., Wiens, D. A., Anandakrishnan, S., Aster, R. C., Gerstoft, P., Bromirski, P. D., et al. (2018). The crust and upper mantle structure of central and West Antarctica from Bayesian inversion of Rayleigh wave and receiver functions. *Journal of Geophysical Research: Solid Earth*, 123, 7824–7849. <https://doi.org/10.1029/2017JB015346>
- Smith, A. G., & Drewry, D. J. (1984). Delayed phase change due to hot asthenosphere causes Transantarctic uplift? *Nature*, 309(5968), 536–538. <https://doi.org/10.1038/309536a0>
- Stern, T., Henrys, S., Okaya, D., Louie, J., Savage, M., Lamb, S., Sato, H., Sutherland, R., Iwasaki, T. (2015). A seismic reflection image for the base of the tectonic plate. *Nature*, 518(7537), 85–88.
- Stern, T., Molnar, P., Okaya, D., & Eberhart-Phillips, D. (2000). Teleseismic P wave delays and modes of shortening the mantle lithosphere beneath South Island, New Zealand. *Journal of Geophysical Research*, 105(B9), 21,615–21,631. <https://doi.org/10.1029/2000JB900166>

- Stern, T., Okaya, D., Kleffmann, S., Scherwath, M., Henrys, S., & Davey, F. (2007). *Geophysical exploration and dynamics of the Alpine fault zone*, *Geophysical Monograph Series* (Vol. 175). Washington, DC: American Geophysical Union. <https://doi.org/10.1029/175GM12>
- Stern, T., Smith, E. G. C., Davey, F. J., & Muirhead, K. J. (1987). Crustal and upper mantle structure of the northwestern North Island, New Zealand, from seismic refraction data. *Geophysical Journal International*, 91(3), 913–936. <https://doi.org/10.1111/j.1365-246x.1987.tb01674.x>
- Stern, T. A., Stratford, W. R., & Salmon, M. L. (2006). Subduction evolution and mantle dynamics at a continental margin: Central North Island, New Zealand. *Reviews of Geophysics*, 44, RG4002. <https://doi.org/10.1029/2005RG000171>
- Stern, T. A., & ten Brink, U. S. (1989). Flexural uplift of the Transantarctic Mountains. *Journal of Geophysical Research*, 94(B8), 10,315–10,330. <https://doi.org/10.1029/JB094iB08p10315>
- Sutherland, R., Spasojevic, S., & Gurnis, M. (2010). Mantle upwelling after Gondwana subduction death explains anomalous topography and subsidence histories of eastern New Zealand and West Antarctica. *Geology*, 38(2), 155–158. <https://doi.org/10.1130/G30613.1>
- Swain, C. J., & Kirby, J. F. (2006). An effective elastic thickness map of Australia from wavelet transforms of gravity and topography using Forsyth's method. *Geophysical Research Letters*, 33, L02314. <https://doi.org/10.1029/2005GL025090>
- ten Brink, U. S., Hackney, R. I., Bannister, S., Stern, T. A., & Makovsky, Y. (1997). Uplift of the Transantarctic Mountains and the bedrock beneath the East Antarctic ice sheet. *Journal of Geophysical Research*, 102(B12), 27,603–27,621. <https://doi.org/10.1029/97JB02483>
- Tenzer, R., & Novak, P. (2013). Effect of crustal density structures on GOCE gravity gradient observables. TAO. *Terrestrial, Atmospheric and Oceanic Sciences*, 24(5), 793–807. [https://doi.org/10.3319/tao.2013.05.08.01\(t\)](https://doi.org/10.3319/tao.2013.05.08.01(t))
- Tenzer, R., Novák, P., Gladkikh, V., & Vajda, P. (2012). Global crust-mantle density contrast estimated from EGM2008, DTM2008, CRUST2. 0, and ICE-5G. *Pure and Applied Geophysics*, 169(9), 1663–1678. <https://doi.org/10.1007/s00024-011-0410-3>
- Tesauro, M., Kaban, M. K., & Cloetingh, S. A. (2012). Global strength and elastic thickness of the lithosphere. *Global and Planetary C*, 90–91, 51–57. <https://doi.org/10.1016/j.gloplacha.2011.12.003>
- Van der Meijde, M., Fadel, I. E. A. M., Ditmar, P., & Hamayun, M. (2015). Uncertainties in crustal thickness models for data sparse environments: A review for South America and Africa. *Journal of Geodynamics*, 84, 1–18. <https://doi.org/10.1016/j.jog.2014.09.013>
- Watts, A. B. (2001). *Isostasy and flexure of the lithosphere*. Cambridge, New York, Melbourne: Cambridge University Press.
- Watts, A. B., & Moore, J. D. P. (2017). Flexural isostasy: Constraints from gravity and topography power spectra. *Journal of Geophysical Research: Solid Earth*, 122, 8417–8430. <https://doi.org/10.1002/2017JB014571>
- Wessel, P., Smith, W. H., Scharroo, R., Luis, J., & Wobbe, F. (2013). Generic mapping tools: Improved version released. *Eos, Transactions American Geophysical Union*, 94(45), 409–410. <https://doi.org/10.1002/2013EO450001>
- Whitehouse, P. L. (2018). Glacial isostatic adjustment modelling: Historical perspectives, recent advances, and future directions. *Earth Surface Dynamics*, 6(2), 401–429. <https://doi.org/10.5194/esurf-6-401-2018>